
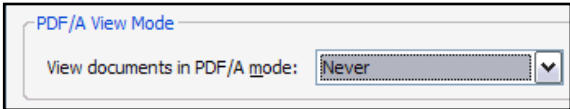
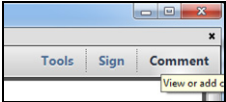
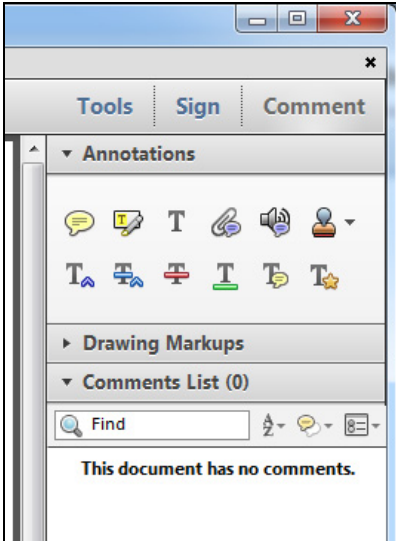










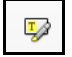


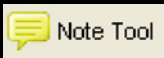

## INSTRUCTIONS ON THE ANNOTATION OF PDF FILES

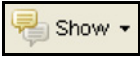
To view, print and annotate your article you will need Adobe Reader version 9 (or higher). This program is freely available for a whole series of platforms that include PC, Mac, and UNIX and can be downloaded from <http://get.adobe.com/reader/>. The exact system requirements are given at the Adobe site: <http://www.adobe.com/products/reader/tech-specs.html>.

*Note: if you opt to annotate the file with software other than Adobe Reader then please also highlight the appropriate place in the PDF file.*

PDF ANNOTATIONS	
Adobe Reader version 9	Adobe Reader version X and XI
<p>When you open the PDF file using Adobe Reader, the Commenting tool bar should be displayed automatically; if not, click on 'Tools', select 'Comment &amp; Markup', then click on 'Show Comment &amp; Markup tool bar' (or 'Show Commenting bar' on the Mac). If these options are not available in your Adobe Reader menus then it is possible that your Adobe Acrobat version is lower than 9 or the PDF has not been prepared properly.</p>  <p>(Mac)</p> <p><b>PDF ANNOTATIONS (Adobe Reader version 9)</b></p> <p>The default for the Commenting tool bar is set to 'off' in version 9. To change this setting select 'Edit   Preferences', then 'Documents' (at left under 'Categories'), then select the option 'Never' for 'PDF/A View Mode'.</p>  <p>(Changing the default setting, Adobe version 9)</p>	<p>To make annotations in the PDF file, open the PDF file using Adobe Reader XI, click on 'Comment'.</p> <p>If this option is not available in your Adobe Reader menus then it is possible that your Adobe Acrobat version is lower than XI or the PDF has not been prepared properly.</p>  <p>This opens a task pane and, below that, a list of all Comments in the text. These comments initially show all the changes made by our copyeditor to your file.</p> 

**HOW TO...**

Action	Adobe Reader version 9	Adobe Reader version X and XI
<b>Insert text</b>	Click the 'Text Edits' button  on the Commenting tool bar. Click to set the cursor location in the text and simply start typing. The text will appear in a commenting box. You may also cut-and-paste text from another file into the commenting box. Close the box by clicking on 'x' in the top right-hand corner.	Click the 'Insert Text' icon  on the Comment tool bar. Click to set the cursor location in the text and simply start typing. The text will appear in a commenting box. You may also cut-and-paste text from another file into the commenting box. Close the box by clicking on 'x'  in the top right-hand corner.
<b>Replace text</b>	Click the 'Text Edits' button  on the Commenting tool bar. To highlight the text to be replaced, click and drag the cursor over the text. Then simply type in the replacement text. The replacement text will appear in a commenting box. You may also cut-and-paste text from another file into this box. To replace formatted text (an equation for example) please <a href="#">Attach a file</a> (see below).	Click the 'Replace (Ins)' icon  on the Comment tool bar. To highlight the text to be replaced, click and drag the cursor over the text. Then simply type in the replacement text. The replacement text will appear in a commenting box. You may also cut-and-paste text from another file into this box. To replace formatted text (an equation for example) please <a href="#">Attach a file</a> (see below).
<b>Remove text</b>	Click the 'Text Edits' button  on the Commenting tool bar. Click and drag over the text to be deleted. Then press the delete button on your keyboard. The text to be deleted will then be struck through.	Click the 'Strikethrough (Del)' icon  on the Comment tool bar. Click and drag over the text to be deleted. Then press the delete button on your keyboard. The text to be deleted will then be struck through.
<b>Highlight text/ make a comment</b>	Click on the 'Highlight' button  on the Commenting tool bar. Click and drag over the text. To make a comment, double click on the highlighted text and simply start typing.	Click on the 'Highlight Text' icon  on the Comment tool bar. Click and drag over the text. To make a comment, double click on the highlighted text and simply start typing.
<b>Attach a file</b>	Click on the 'Attach a File' button  on the Commenting tool bar. Click on the figure, table or formatted text to be replaced. A window will automatically open allowing you to attach the file. To make a comment, go to 'General' in the 'Properties' window, and then 'Description'. A graphic will appear in the PDF file indicating the insertion of a file.	Click on the 'Attach File' icon  on the Comment tool bar. Click on the figure, table or formatted text to be replaced. A window will automatically open allowing you to attach the file. A graphic will appear indicating the insertion of a file.
<b>Leave a note/ comment</b>	Click on the 'Note Tool' button  on the Commenting tool bar. Click to set the location of the note on the document and simply start typing. <u>Do not use this feature to make text edits.</u>	Click on the 'Add Sticky Note' icon  on the Comment tool bar. Click to set the location of the note on the document and simply start typing. <u>Do not use this feature to make text edits.</u>

HOW TO...		
Action	Adobe Reader version 9	Adobe Reader version X and XI
<b>Review</b>	To review your changes, click on the 'Show' button  on the Commenting tool bar. Choose 'Show Comments List'. Navigate by clicking on a correction in the list. Alternatively, double click on any mark-up to open the commenting box.	Your changes will appear automatically in a list below the Comment tool bar. Navigate by clicking on a correction in the list. Alternatively, double click on any mark-up to open the commenting box.
<b>Undo/delete change</b>	To undo any changes made, use the right click button on your mouse (for PCs, Ctrl-Click for the Mac). Alternatively click on 'Edit' in the main Adobe menu and then 'Undo'. You can also delete edits using the right click (Ctrl-click on the Mac) and selecting 'Delete'.	To undo any changes made, use the right click button on your mouse (for PCs, Ctrl-Click for the Mac). Alternatively click on 'Edit' in the main Adobe menu and then 'Undo'. You can also delete edits using the right click (Ctrl-click on the Mac) and selecting 'Delete'.

#### SEND YOUR ANNOTATED PDF FILE BACK TO ELSEVIER

Save the annotations to your file and return as instructed by Elsevier. Before returning, please ensure you have answered any questions raised on the Query Form and that you have inserted all corrections: later inclusion of any subsequent corrections cannot be guaranteed.

#### FURTHER POINTS

- Any (grey) halftones (photographs, micrographs, etc.) are best viewed on screen, for which they are optimized, and your local printer may not be able to output the greys correctly.
- If the PDF files contain colour images, and if you do have a local colour printer available, then it will be likely that you will not be able to correctly reproduce the colours on it, as local variations can occur.
- If you print the PDF file attached, and notice some 'non-standard' output, please check if the problem is also present on screen. If the correct printer driver for your printer is not installed on your PC, the printed output will be distorted.

# The Ubiquitin Ligase FBXW7 Modulates Leukemia-Initiating Cell Activity by Regulating MYC Stability

Bryan King,<sup>1</sup> Thomas Trimarchi,<sup>1</sup> Linsey Reavie,<sup>1,4</sup> Luyao Xu,<sup>5</sup> Jasper Mullenders,<sup>1</sup> Panagiotis Ntziachristos,<sup>1</sup> Beatriz Aranda-Orgilles,<sup>1</sup> Arianne Perez-Garcia,<sup>5</sup> Junwei Shi,<sup>6</sup> Christopher Vakoc,<sup>6</sup> Peter Sandy,<sup>7</sup> Steven S. Shen,<sup>1,3</sup> Adolfo Ferrando,<sup>4</sup> and Iannis Aifantis<sup>1,2,\*</sup>

<sup>1</sup>Howard Hughes Medical Institute and NYU Cancer Institute

<sup>2</sup>Department of Pathology

<sup>3</sup>Center for Health Informatics and Bioinformatics

NYU School of Medicine, New York, NY 10016, USA

<sup>4</sup>Department of Experimental Oncology, European Institute of Oncology, 20139 Milan, Italy

<sup>5</sup>Institute for Cancer Genetics, Columbia University, New York, NY 10027, USA

<sup>6</sup>Cold Spring Harbor Laboratory, Cold Spring Harbor, New York, NY 11224, USA

<sup>7</sup>Constellation Pharmaceuticals, Cambridge, MA 02142, USA

\*Correspondence: [iannis.aifantis@nyumc.org](mailto:iannis.aifantis@nyumc.org)

<http://dx.doi.org/10.1016/j.cell.2013.05.041>

## SUMMARY

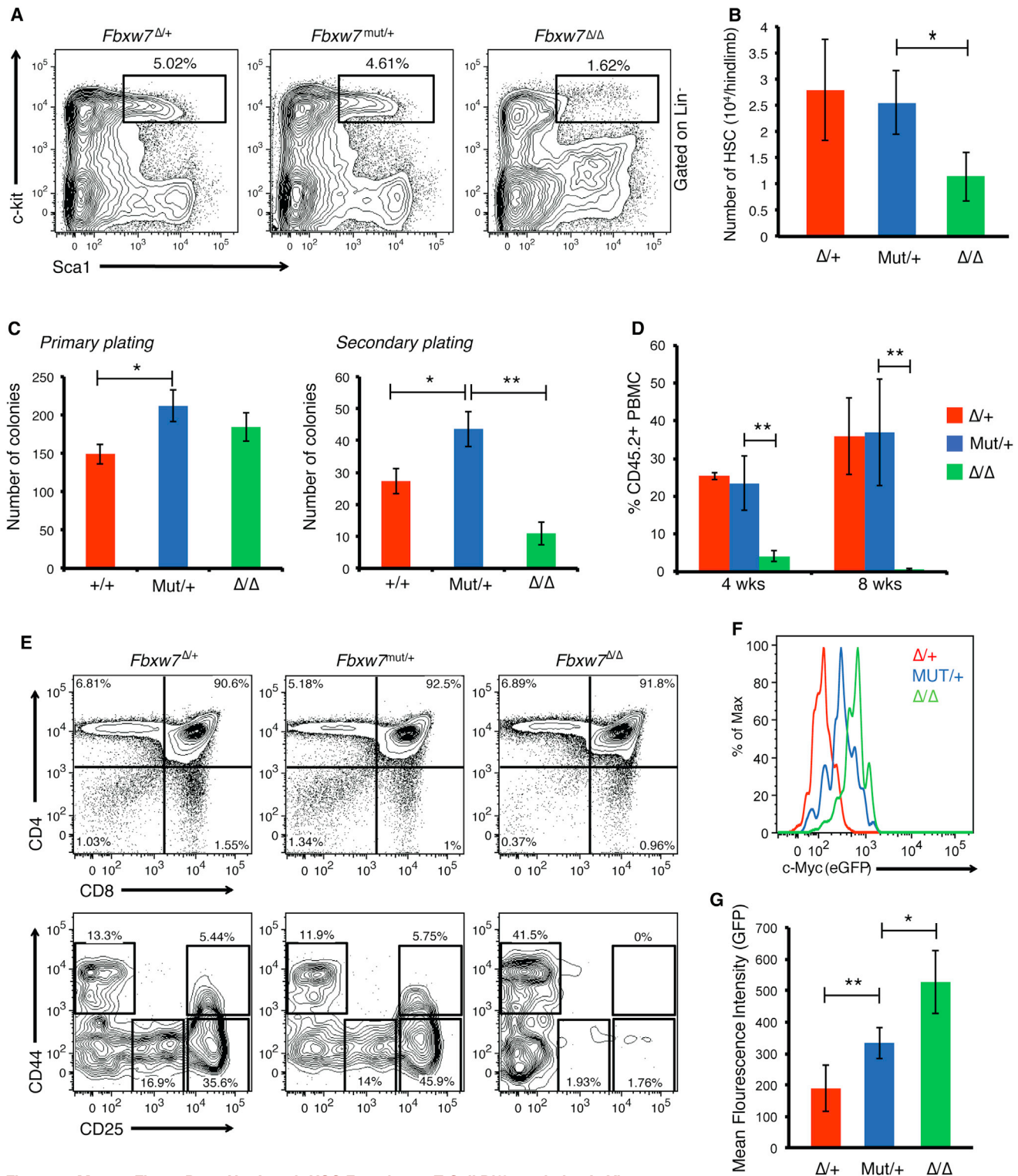
Sequencing efforts led to the identification of somatic mutations that could affect the self-renewal and differentiation of cancer-initiating cells. One such recurrent mutation targets the binding pocket of the ubiquitin ligase Fbxw7. Missense FBXW7 mutations are prevalent in various tumors, including T cell acute lymphoblastic leukemia (T-ALL). To study the effects of such lesions, we generated animals carrying regulatable *Fbxw7* mutant alleles. Here, we show that these mutations specifically bolster cancer-initiating cell activity in collaboration with Notch1 oncogenes but spare normal hematopoietic stem cell function. We were also able to show that FBXW7 mutations specifically affect the ubiquitylation and half-life of c-Myc protein, a key T-ALL oncogene. Using animals carrying c-Myc fusion alleles, we connected Fbxw7 function to c-Myc abundance and correlated c-Myc expression to leukemia-initiating activity. Finally, we demonstrated that small-molecule-mediated suppression of MYC activity leads to T-ALL remission, suggesting an effective therapeutic strategy.

## INTRODUCTION

As next-generation sequencing studies identify novel genetic lesions in cancer, it becomes evident that mutations affecting key regulators of diverse cellular processes ranging from metabolism to protein stability are somatically selected in cancer cells (Downing et al., 2012; Hodis et al., 2012; Zhang et al., 2012). Presumably, these mutations are selected for because they bestow cells with tumorigenic properties while sparing their essential

functions. Heterozygosity of such mutations further complicates their study, given that it suggests that either small protein expression differences can have profound outcomes or missense mutants might have neomorphic and/or dominant-negative functions. Moreover, mutations rarely act in isolation but, instead, act in a synergistic manner with additional oncogenic lesions. Thus, it is vital to study the impact of somatic missense mutations with genetic models closely mimicking the corresponding human cancer genotypes and to consider the in vivo effects of mutational cooperation.

FBXW7 is mutated in a significant portion of human tumors, including approximately 20% of patients with T cell acute lymphoblastic leukemia (T-ALL) (Akhoondi et al., 2007; O'Neil et al., 2007; Thompson et al., 2007). Fbxw7 is a constituent of the SCF (Skp1-Cul1-F box) ubiquitin ligase complex that controls the degradation and half-life of key cellular regulators, including Cyclin E, Notch1, c-Myc, and Mcl1 (Crusio et al., 2010; Wang et al., 2012). Mutations in FBXW7 are predominantly heterozygous and cluster within the WD40 substrate-binding domain, specifically affecting three highly conserved arginine residues (Nash et al., 2001). Although the outcome of expressing these particular mutations in somatic tissues remains unknown, monoallelic deletion of *Fbxw7* in the hematopoietic system fails to induce leukemia. Although complete deletion can lead to T-ALL establishment, albeit with low penetrance (Matsuoka et al., 2008), the prevailing phenotype of *Fbxw7* loss is a progressive bone marrow (BM) failure that eventually leads to fatal anemia. These findings imply that FBXW7 missense mutants are not simply "dead" alleles and could behave differently in normal and malignant cells. Accordingly, nonsense FBXW7 mutations are relatively rare in T-ALL (O'Neil et al., 2007; Thompson et al., 2007). Although the biochemical mechanism behind FBXW7 mutations in T-ALL remains unclear, our group and others have found that these lesions affect the stability of Notch1, the main T-ALL oncogene, which is mutated in approximately half of T cell leukemia patients (Weng et al., 2004). In agreement with



**Figure 1. Mutant *Fbxw7* Does Not Impair HSC Function or T Cell Differentiation In Vivo**

(A and B) Representative fluorescence-activated cell sorting (FACS) plots showing the frequency of Lin<sup>-</sup>c-kit<sup>+</sup>Sca-1<sup>+</sup> (LSK) BM cells from *Fbxw7*<sup>Δ/+</sup>, *Fbxw7*<sup>mut/+</sup>, or *Fbxw7*<sup>Δ/Δ</sup> mice 8 weeks after pl:pC injection (A) and the number of phenotypic LT-HSCs (CD150<sup>+</sup>CD48<sup>-</sup> LSK) recovered (B).

(C) Primary and secondary colonies derived from LSKs sorted from the BM of the indicated genotype.

(D) Frequency of CD45.2<sup>+</sup> donor-derived peripheral blood mononuclear cells (PBMCs) in lethally irradiated recipient mice transplanted with 5 × 10<sup>5</sup> total BMMCs from either *Fbxw7*<sup>F/F</sup>*Mx1Cre*<sup>-/-</sup>, *Fbxw7*<sup>mut/+</sup>*Mx1Cre*<sup>-/-</sup>, or *Fbxw7*<sup>F/F</sup>*Mx1Cre*<sup>-/-</sup> mice (CD45.2<sup>+</sup>) mixed at a 1:1 ratio with WT BMMCs (CD45.1<sup>+</sup>) at 4 and 8 weeks after transplant.

FACS profiling of thymocytes from *Fbxw7*<sup>Δ/+</sup>, *Fbxw7*<sup>mut/+</sup>, or *Fbxw7*<sup>Δ/Δ</sup> mice analyzed 4 weeks after pl:pC injections.

(legend continued on next page)

this notion, approximately 25% of *NOTCH1* mutations in T-ALL truncate the protein deleting the conserved degron sequence recognized by Fbxw7. Similar mutations in either *NOTCH1* or *FBXW7* genes are also found in a larger number of additional cancer types, including marginal B cell lymphoma and melanoma (Hodis et al., 2012; Rossi et al., 2012), making the thorough understanding of their function critical for future therapies.

To study the transforming effects of such missense mutations in vivo, we have generated mice that carry Cre-inducible *Fbxw7* heterozygous mutants, mimicking the most common substitution found in human T-ALL (R465C). Interestingly, in contrast to previous knockout models, these mutations did not compromise normal hematopoietic stem cell (HSC) function but lead to a marked increase in the proportion of leukemia-initiating cells (LICs) due to the stabilization of the Fbxw7 substrate c-Myc. Using animals expressing fluorescent c-Myc fusion proteins (*Myc<sup>GFP</sup>*), we were able to show a perfect correlation between c-Myc stabilization and leukemia-initiating activity. Moreover, we were able to demonstrate that c-Myc deletion in established T-ALL specifically ablates LICs and that the inhibition of c-Myc induction with small-molecule BET inhibitors targeting Brd4 (Filippakopoulos et al., 2010; Zuber et al., 2011) can suppress the growth of mouse and human T-ALL cells. Finally, direct c-Myc and Brd4 gene targets in T-ALL were identified genome wide and suggested an intriguing transcriptional cooperation between these factors and Notch1. Altogether, these studies identify *FBXW7<sup>R465C</sup>* as a unique type of somatic mutation, given that it has the ability to specifically alter cancer-initiating cell activity without consequence to normal stem cell differentiation.

## RESULTS

### Generation of Inducible Knockin Models of FBXW7 Missense Mutations

To test the function of *FBXW7* mutations in vivo, we targeted the most common recurrent mutation, an arginine-to-cysteine change at position 465 (468 in the mouse) (Aifantis et al., 2008). Given that mice that harbor a similar germline mutation in *Fbxw7* die perinatally because of defects in lung development (Davis et al., 2011), we generated mutant alleles that could be conditionally activated with the Cre-lox system. Using homologous recombination, we generated an R468C mutation in the endogenous *Fbxw7* gene and inserted a lox-STOP-lox cassette in the upstream intron, thereby functioning as a null allele prior to recombination and as a mutant in all lineages where Cre is activated (Figure S1A available online). *Fbxw7<sup>R468Neo/+</sup>* pups were born and developed normally, yet *Fbxw7<sup>R468Neo/R468Neo</sup>* mice were never represented, which was consistent with reports that *Fbxw7*-null mice die in utero (Tsunematsu et al., 2004). Mice were crossed to the pl:pC-inducible Mx1-Cre allele (Kühn et al., 1995). Recombination was observed in the genomic DNA of BM cells, and the mutation could be detected in messenger RNA (mRNA) (Figures S1B–S1C) after pl:pC treat-

ment. Alternatively, to study the effect of the exact human R465C mutation, we introduced an exogenous human *FBXW7<sup>R465C</sup>* complementary DNA (cDNA) (with an N-terminal FLAG tag) in the ubiquitously expressed elongation factor 1 alpha (*Eef1a1*) locus (Klinakis et al., 2009). As with the endogenous mouse *Fbxw7* mutant, this targeting positioned a lox-STOP-lox cassette upstream of the mutant cDNA for conditional activation (Figure S1D). Upon Cre induction, we could detect robust expression of a 110 kDa protein by FLAG immunoblot in lysates from primary tissues (Figure S1E). Furthermore, the mutant human Fbxw7 was functional and incorporated into the SCF complex, whereas other components (Skp1 and Cul1) could be coimmunoprecipitated (data not shown). As will become evident from the following studies, both alleles (*Fbxw7<sup>R468</sup>* and *Eef1a1<sup>mutW7</sup>*) yield similar phenotypes. Most of the presented studies will focus on the *Fbxw7<sup>R468</sup>* endogenous allele (referred as *Fbxw7<sup>mut</sup>*).

### FBXW7 Mutations Do Not Affect Normal HSC and Progenitor Differentiation

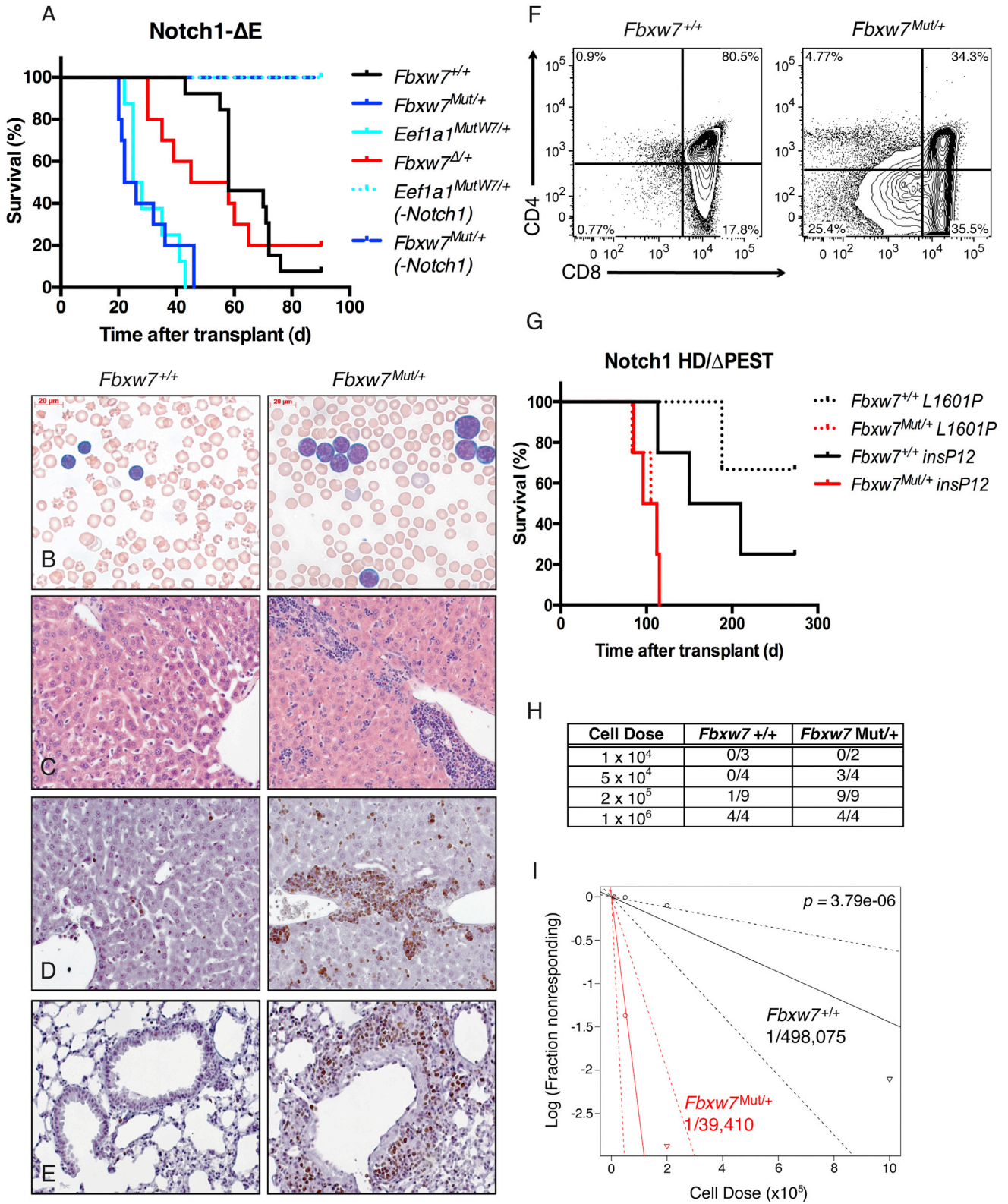
Previous studies have shown that conditional deletion of *Fbxw7* in the adult hematopoietic system leads to a rapid depletion of HSCs and T cell progenitors (Matsuoka et al., 2008; Thompson et al., 2008). Given that HSCs provide a long-lived reservoir of cells with an inherent capacity for self-renewal, it has been hypothesized that many of the oncogenic lesions found in hematopoietic malignancies might arise in HSCs or multipotent progenitors (Francis and Richardson, 2007; Mohrin et al., 2010). However, this presents a paradox for *FBXW7* mutations in particular, given that these mutations could be deleterious for normal hematopoiesis and selected against prior to transformation. To test the possibility that heterozygous *Fbxw7* mutations might be tolerated differently than deletion of one or both alleles, we assessed HSC function in *Fbxw7<sup>F/+</sup>Mx1-Cre<sup>+</sup>* (*Fbxw7<sup>Δ/+</sup>*), *Fbxw7<sup>mut/+</sup>Mx1-Cre<sup>+</sup>*, and *Fbxw7<sup>F/F</sup>Mx1-Cre<sup>+</sup>* mice (*Fbxw7<sup>Δ/Δ</sup>*). As expected, the frequency and absolute number of HSCs (Lin<sup>-</sup>Sca1<sup>+</sup>c-kit<sup>+</sup>CD150<sup>+</sup>CD48<sup>-</sup>) was significantly lower in *Fbxw7<sup>Δ/Δ</sup>* in comparison to *Fbxw7<sup>Δ/+</sup>* BM. However, there was no decrease in phenotypic HSCs observed in *Fbxw7<sup>mut/+</sup>* mice (Figures 1A–1B). Also, *Fbxw7<sup>mut/+</sup>* HSCs were more functionally competent than *Fbxw7<sup>Δ/Δ</sup>*, given that they generated a greater number of colonies in colony-forming assays (Figure 1C) and reconstituted recipient mice to the same extent as *Fbxw7<sup>Δ/+</sup>* donors upon competitive BM transplantation (Figure 1D). Moreover, the depletion of early T cell progenitors typically seen in *Fbxw7<sup>Δ/Δ</sup>* thymii was also absent in *Fbxw7<sup>mut/+</sup>* mice (Figure 1E), demonstrating that the mutant progenitors could colonize the *Fbxw7*-deficient thymus and differentiate normally.

*Fbxw7*-deficient HSCs fail to self-renew primarily because of an aberrant accumulation of c-Myc protein (Reavie et al., 2010). To test whether differential c-Myc abundance could account for the inability of the mutant allele to affect hematopoiesis, we determined the level of c-Myc protein in HSC of each

(E and F) Histogram (E) and calculated mean fluorescence intensity (F) of GFP measured by FACS in LT-HSCs from mice in (A) and (B) expressing a c-Myc:GFP fusion (*Myc<sup>GFP/+</sup>*) allele.

Error bars in (B), (C), (D), and (G) indicate mean ± SD. \*p < 0.05; \*\*p < 0.01.

See also Figure S1.



(legend on next page)

genotype by crossing the *Fbxw7<sup>mut</sup>* and *Fbxw7<sup>F/F</sup>* Mx1-Cre strains to a mouse expressing a c-Myc:GFP fusion from the endogenous *Myc* locus (*Myc<sup>GFP</sup>*) (Huang et al., 2008). Intriguingly, the level of c-Myc stabilization in mutant HSCs was significantly greater than that of *Fbxw7<sup>Δ/+</sup>* but still lower than that observed in *Fbxw7*-deficient HSCs (Figures 1F–1G). Altogether, these data imply that the intermediate levels of c-Myc stabilization resulting from a heterozygous *Fbxw7* mutation are tolerated in HSCs, whereas the level of c-Myc in *Fbxw7*-deficient HSCs surpasses a threshold that is incompatible self-renewal.

### FBXW7 and NOTCH1 Mutations Cooperate for the Induction of Aggressive Leukemia

Although mutations in *Fbxw7* are highly prevalent and implicated in the pathogenesis of T-ALL (O'Neil et al., 2007; Thompson et al., 2007), it is unknown whether these mutations are sufficient for leukemia induction in vivo. To address this question, a cohort of *Fbxw7<sup>mut/+</sup>* or *Eef1a1<sup>mutW7/+</sup>* mice were monitored periodically by peripheral blood analysis for up to 18 months. Surprisingly, none of these mutant mice ever exhibited elevated white blood cell counts in comparison to their wild-type (WT) littermates or developed leukemia spontaneously (Figure 2A). Moreover, no other tumors or developmental defects were observed when a single mutant allele was activated in early-stage embryos with Ella-Cre (data not shown). Next, we tested whether *Fbxw7* mutations would act synergistically with other known T-ALL oncogenes. *FBXW7* mutations frequently co-occur with *NOTCH1* heterodimerization domain (HD) mutations in human T-ALL (Grabher et al., 2006). This scenario was modeled in vivo by retroviral expression of Notch1ΔE, a truncated form of Notch1 that is constitutively cleaved in a ligand-independent manner (Aster et al., 1997) on an *Fbxw7<sup>+/+</sup>*, *Fbxw7<sup>Δ/+</sup>*, *Fbxw7<sup>mut/+</sup>*, or *Eef1a1<sup>mutW7/+</sup>* background. Although all four cohorts eventually succumbed to T-ALL, the cohorts transplanted with either *Fbxw7* mutant developed leukemia at a much shorter latency in comparison to the *Fbxw7<sup>+/+</sup>* and the *Fbxw7<sup>Δ/+</sup>* groups (Figure 2A). The median survival of the *Fbxw7<sup>mut/+</sup>* and *Eef1a1<sup>mutW7/+</sup>* cohorts was identical. Mice from each group were analyzed at 21 days after transplant in order to evaluate leukemia progression. The mutant cohorts presented with a higher proportion of leukemic blasts, notably larger in size in comparison to their WT counterparts, in the peripheral blood and heavier infiltration of peripheral tissues (Figures 2B and 2C). In addition, a

greater proportion of these blasts were actively cycling, as exhibited by more prominent Ki67 staining (Figures 2D and 2E). Because the extent of maturation of T-ALL often correlates with a poorer prognosis (Ferrando and Look, 2003; Zhang et al., 2012), the expression of surface markers corresponding to different stages of physiological T cell development was compared between genotypes. A noticeable trend in decreased CD4 and, to a lesser extent, CD8 surface expression was observed in the *Fbxw7* mutant leukemias (Figure 2F), suggesting a more immature (and potentially aggressive) phenotype. Given that Notch1 is an *Fbxw7* substrate, we repeated the presented leukemia-induction experiments using human Notch1-ΔPEST mutants (Chiang et al., 2008), which are lacking the C-terminal region bound by *Fbxw7*. As seen in Figure 2G, *Fbxw7<sup>mut/+</sup>* Notch1<sup>ΔPEST</sup> tumors also developed with significantly shorter latency, suggesting that additional Notch stabilization alone could not explain the aggressiveness of the disease.

Initial attempts to serially transplant the disease revealed that the *Fbxw7<sup>mut</sup>* leukemias were more efficient in generating secondary tumors (Figure 2H). Thus, we hypothesized that the frequency of LICs might be higher within the *Fbxw7<sup>mut</sup>* leukemia. To quantify the LIC frequencies in *Fbxw7* mutant or WT T-ALL, we transplanted equivalent numbers of GFP<sup>+</sup> cells sorted from leukemias arising from either genotype into secondary recipients at a range of doses from 10<sup>4</sup>–10<sup>6</sup> cells per recipient. All of the mice transplanted with 10<sup>6</sup> cells, regardless of *Fbxw7* status, eventually developed leukemia. However, the frequency of leukemia in mice that received 2 × 10<sup>5</sup> or 5 × 10<sup>4</sup> cells was significantly higher between the *Fbxw7* mutant cohorts (100% versus 11% and 75% versus 0%, respectively) (Figure 2H). Using limiting dilution analysis (Buchstaller et al., 2012), we calculated that the LIC frequency within the *Fbxw7* mutant T-ALL was more than 10-fold higher than in *Fbxw7* WT T-ALL (Figure 2I).

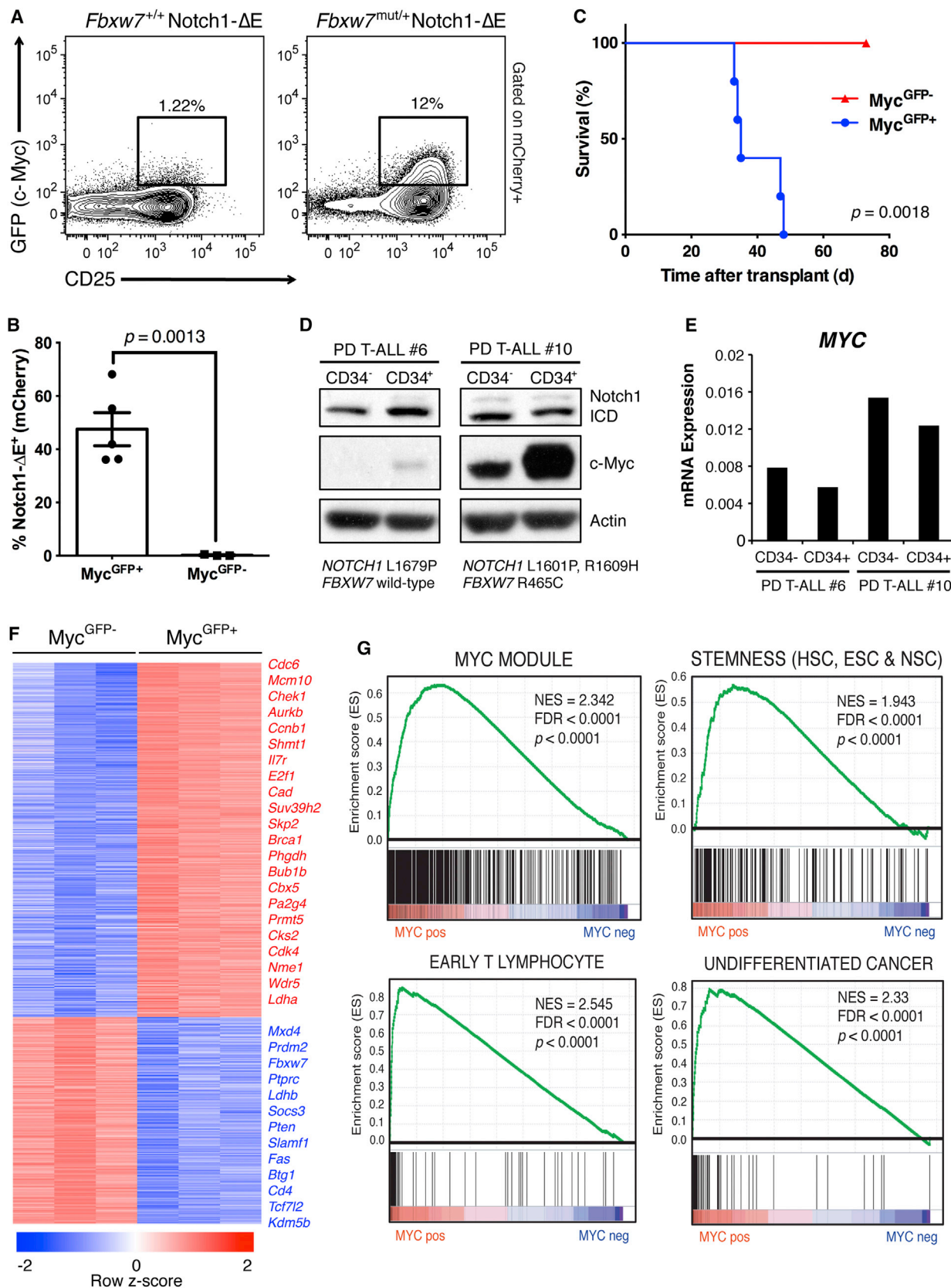
### FBXW7 Mutations Do Not Lead to Genomic Instability or Cooperate with p53 Loss

Previous studies observed genomic instability in human cancer cells when *FBXW7* was deleted (Grim et al., 2012; Rajagopalan et al., 2004). To test whether chromosomal abnormalities were contributing to leukemia development in vivo, we utilized metaphase fluorescent in situ hybridization (mFISH) to karyotype *Fbxw7* mutant leukemias. However, the vast majority of tumor cells had a normal karyotype (Figure S2A). To test for smaller

**Figure 2. *Fbxw7* Mutations Accelerate NOTCH1-Induced T-ALL and Expand the Number of LICs**

- (A) A Kaplan-Meier (K-M) curve representing morbidity in recipient mice transplanted with BM from *Fbxw7<sup>mut/+</sup>*, *Eef1a1<sup>mutW7/+</sup>*, *Fbxw7<sup>Δ/+</sup>*, or *Fbxw7<sup>+/+</sup>* transduced with a Notch1ΔE ires GFP retrovirus. As a control, mice transplanted with *Fbxw7<sup>mut/+</sup>* or *Eef1a1<sup>mutW7/+</sup>* cells not expressing a Notch1ΔE (–Notch1) are shown (Mantel-Cox log rank test; *Fbxw7<sup>mut/+</sup>* versus *Fbxw7<sup>+/+</sup>*, p < 0.0001; *Fbxw7<sup>mut/+</sup>* versus *Fbxw7<sup>Δ/+</sup>*, p = 0.0056; *Fbxw7<sup>Δ/+</sup>* versus *Fbxw7<sup>+/+</sup>*, p = 0.5617).
- (B–E) Peripheral blood and organs were harvested 3 weeks after transplant and prepared for histology.
- (B) A Wright-Giemsa stain of peripheral blood.
- (C) Hematoxylin and eosin staining of the liver.
- (D and E) Ki67 staining of the liver and lung.
- (F) Representative FACS plots depicting CD4 and CD8 expression on either *Fbxw7<sup>mut/+</sup>* or *Fbxw7<sup>+/+</sup>* GFP<sup>+</sup> cells in the peripheral blood of recipients.
- (G) A K-M curve representing morbidity in recipient mice transplanted with BM from *Fbxw7<sup>mut/+</sup>* or *Fbxw7<sup>+/+</sup>* mice transduced with retroviruses expressing mutant, truncated forms of Notch1 lacking a C-terminal PEST domain, and bearing *NOTCH1* HD (L1601P and insP12) mutations (L1601P, p = 0.0177; insP12, p = 0.0266).
- (H) A fraction of secondary recipients that developed leukemia when transplanted with limiting dilutions of GFP<sup>+</sup> splenocytes sorted from either *Fbxw7* WT or mutant T-ALL mice.
- (I) A log-log plot and leukemia initiating cell frequency calculated by extreme limiting dilution analysis. Red, *Fbxw7<sup>mut/+</sup>* (1/39,410); black, *Fbxw7<sup>+/+</sup>* (1/498,075). See also Figures S1 and S2.





(legend on next page)

genomic events, we analyzed DNA from leukemic cells by array-comparative genomic hybridization (array CGH). Several *Fbxw7* mutant or WT leukemias were analyzed, and normal tissue from donor mice was used as a reference. Between both groups of samples, the only significant DNA gain or loss consistently found was within the *Tcra* locus (Figure S2B), which was in agreement with the identity and developmental stage of the leukemia. Although neither of these results rule out the possibility of collaborating point mutations, genetic instability is unlikely to be responsible for the more aggressive nature of *Fbxw7* mutant leukemias. In addition to activating mutations in *Notch1*, *Fbxw7* has been genetically associated with the inactivation of p53 in a number of tumor models (Grim et al., 2012; Onoyama et al., 2007). To determine whether loss of p53 could collaborate with our *Fbxw7* mutant allele, we transduced *Fbxw7*<sup>+/+</sup>, *Fbxw7*<sup>mut/+</sup>, or *Fbxw7*<sup>Δ/Δ</sup> BM with a retroviral small hairpin RNA (shRNA) targeting *Trp53*. The WT or *Fbxw7*<sup>Δ/Δ</sup> donors generated tumors in recipient animals with a time of onset and disease phenotype that coincided with the previous genetic models (Figure S2C). However, the latency of leukemia development was not decreased by the mutation of *Fbxw7*, despite the efficient silencing of *Trp53* (Figure S2D). Therefore, there is a clear disparity between *Fbxw7*-null and *Fbxw7*<sup>R465C</sup> mutants in the requirement for p53 inactivation. Moreover, unlike *NOTCH1*, *TP53* mutations are not enriched in *FBXW7* mutant human T-ALL (Zhang et al., 2012), thus supporting our findings with the *Fbxw7*<sup>mut</sup> animal models.

### FBXW7 Mutations Affect c-Myc Protein Half-Life and Ubiquitylation

Having ruled out genomic instability, we sought to determine the mechanism by which *Fbxw7* mutations confer a greater leukemia initiating capacity to cells uniformly expressing a *Notch1* oncogene. The protein half-life of a panel of known substrates was measured in either *Fbxw7* WT or mutant *Notch1* T-ALL cells *ex vivo* (Figure S3A). Of the substrates tested, we noted moderate stabilization of *Notch1* and *Srebp1* and a very consistent and significant stabilization of c-Myc (Figure S3A). *Myc* has an essential role in cell growth and self-renewal (Eilers and Eisenman, 2008; Murphy et al., 2005) and has previously been implicated in the pathogenesis of T-ALL as a transcriptional target of *Notch1* (Palomero et al., 2006; Sharma et al., 2006). Thus, we focused on the putative mechanisms of c-Myc stabilization by the mutant *Fbxw7* allele. In an *in vitro* ubiquitylation assay, the R465C mutation renders *Fbxw7* incapable of ubiquitylating c-Myc (Figure S3B). Given that SCF-*Fbxw7* complexes have been shown

to dimerize in certain conditions (Welcker and Clurman, 2007), we hypothesized that *Fbxw7* mutations could affect the ability of *Fbxw7*<sup>mut</sup>:*Fbxw7*<sup>WT</sup> heterodimers to bind and ubiquitylate c-Myc. To test this hypothesis, we expressed either *Fbxw7*<sup>WT</sup> or *Fbxw7*<sup>R465C</sup> bearing unique epitope tags, isolated dimers, and quantified binding to endogenous c-Myc. Although a robust interaction with c-Myc was detected in the WT:WT dimers, binding to MUT:WT dimers was significantly decreased (Figure S3C). MUT:MUT *Fbxw7* homodimers failed to bind detectable levels of c-Myc.

### Fbw7-Regulated c-Myc Protein Expression Specifically Marks LSCs In Vivo

To track c-Myc protein levels during leukemia progression *in vivo*, we transplanted either *Fbxw7*<sup>+/+</sup>*Myc*<sup>GFP/+</sup> or *Fbxw7*<sup>mut/+</sup>*Myc*<sup>GFP/+</sup> BM cells transduced with a *Notch1*ΔE-ires-mCherry retroviral vector. Because *Myc* is a transcriptional target of *Notch1* (Palomero et al., 2006), we expected that the *Notch1*ΔE-transduced population would uniformly express high levels of *Myc*<sup>GFP</sup>. However, at earlier time points, *Notch1*ΔE<sup>+</sup> cells that had detectable levels of c-Myc were virtually absent from circulation (Figure S4A) and rare in the spleen (Figure 3A). Strikingly, this population was typically 10-fold larger in the *Fbxw7* mutant leukemia (Figure 3A). Costaining for T cell surface markers revealed that *Myc*<sup>GFP</sup> expression was highest in the CD4<sup>+</sup>CD8<sup>-</sup>CD25<sup>hi</sup> (DN3) and ISP8 (CD4<sup>-</sup>CD8<sup>+</sup>TCRb<sup>low</sup>) fractions but was undetectable in CD4<sup>+</sup>CD8<sup>+</sup> (DP) cells. Notably, the *Myc*<sup>GFP+</sup> leukemic cells also had elevated IL-7Rα expression (Figure S4B). As the leukemia progressed, the *Myc*<sup>GFP+</sup> population became more abundant, but it never achieved a majority (Figure S4C). Interestingly, between hematopoietic and lymphoid organs, the highest frequency of *Myc*<sup>GFP+</sup> cells was consistently observed in the spleen (Figure S4D).

To determine whether the *Myc*<sup>GFP+</sup> population was enriched in LIC activity, 10<sup>5</sup> *Notch1*ΔE<sup>+</sup>*Myc*<sup>GFP+</sup> and *Notch1*ΔE<sup>+</sup>*Myc*<sup>GFP-</sup> cells were sorted from the spleen of leukemic mice (Figures S4E–S4F) and transplanted into secondary recipients. Two weeks after transplant, the cohort transplanted with *Myc*<sup>GFP+</sup> cells had significantly greater numbers of leukemic cells in peripheral blood (Figure 3B). More importantly, the cohort transplanted with *Myc*<sup>GFP-</sup> cells exhibited 100% leukemia-free survival, whereas the *Myc*<sup>GFP+</sup> cohort all succumbed to T-ALL by 6 weeks after transplant (Figure 3C). Importantly, secondary leukemias arising from the *Myc*<sup>GFP+</sup> cohort re-established the heterogeneity of the primary tumor, including both *Myc*<sup>GFP+</sup> and *Myc*<sup>GFP-</sup> cells (Figure S4G), demonstrating that *Myc*<sup>GFP+</sup> cells

### Figure 3. Myc Protein Stability and Expression Defines Leukemia-Initiating Potential in T-ALL

*Fbxw7*<sup>mut/+</sup>*Myc*<sup>GFP/+</sup> or *Fbxw7*<sup>+/+</sup>*Myc*<sup>GFP/+</sup> BM was transduced with *Notch1*ΔE-ires-mCherry and transplanted into lethally-irradiated recipients.

(A) c-Myc<sup>GFP</sup> in mCherry<sup>+</sup> splenocytes derived from either donor measured by FACS 4 weeks after transplant (the frequency of mCherry<sup>+</sup> cells expressing both c-Myc<sup>GFP</sup> and CD25 is shown). *Fbxw7*<sup>+/+</sup> mCherry<sup>+</sup> splenocytes from leukemic mice were sorted on the basis of c-Myc<sup>GFP</sup> expression and transplanted into sublethally irradiated recipients.

(B and C) Frequency of mCherry<sup>+</sup> PBMC 3 weeks after transplant (B) and the survival (C) of secondary recipients.

(D and E) Immunoblot for c-Myc and intracellular *Notch1* (ICD) (D) and quantitative RT-PCR (qRT-PCR) analysis for *MYC* transcript (normalized to *GAPDH*) (E) in two independent primary human T-ALL xenografts sorted on the basis of CD34 expression. *NOTCH1* and *FBXW7* mutational status is shown for each patient.

(F) A heat map depicting differentially expressed genes (fold change > 2, p < 0.05) in *Notch1*ΔE<sup>+</sup>c-Myc<sup>GFP+</sup> versus *Notch1*ΔE<sup>+</sup>c-Myc<sup>GFP-</sup> T-ALL cells sorted from the spleen of three individual mice.

(G) Selected expression signatures found to be enriched in c-Myc<sup>GFP+</sup> population as determined by GSEA.

See also Figures S3 and S4.

can self-renew and differentiate—the defining properties of a cancer stem cell. Altogether, these data define c-Myc protein abundance a bona fide LIC marker in a T-ALL mouse model and suggest that this population is heavily dependent on Fbxw7 activity. To test whether this observation translates to human T-ALL, CD34<sup>+</sup> populations enriched for T-ALL LICs (Armstrong et al., 2009) were purified from human patient samples that carry NOTCH1 and FBXW7 mutations. In agreement with the mouse data, non-LIC subsets expressed significantly lower levels of c-Myc protein in comparison to the CD34<sup>+</sup> fraction (Figure 3D) despite no increase in MYC mRNA (Figure 3E) or cleaved Notch1. c-Myc levels were higher in samples carrying FBXW7 mutations, further supporting the notion that missense FBXW7 mutations augment c-Myc protein stability in T-ALL.

### T-ALL LICs Are Defined by a Myc Gene Expression Signature

To study this subpopulation enriched in T-ALL LIC activity further, we sought to determine its underlying molecular signature using gene expression analysis. Total RNA was isolated from either Myc<sup>GFP+</sup> or Myc<sup>GFP-</sup> leukemic cells, and gene expression was determined by microarray analysis (Figure 3F). The most represented group among the top upregulated genes included those involved in the mitotic phase of the cell cycle (*Cdc6*, *Ccnb1*, *Chek1*, *Aurkb*, and *Brca1*) and, as expected, transcriptional targets of c-Myc (*Cad*, *Suv39h2*, *Bcat1*, and *Pa2g4*) (Kim et al., 2008; Margolin et al., 2009). Also, many genes encoding cell-surface markers (*Fas*, *Slamf1*, *Il7r*, and *Cd4*), which may be helpful for further thorough dissection of the LIC population, differed significantly at the mRNA level between the two populations. Gene set enrichment analysis (GSEA) was performed in order to identify gene modules that are enriched within the Myc<sup>GFP+</sup> population (Figure 3G). Gene sets pertaining to stem cell identity, including common genes upregulated in adult and embryonic stem cell (ESC) populations, as well as a set of c-Myc-regulated genes in both ESCs and human cancers (Kim et al., 2008), were highly enriched (Figure 3F). Gene sets associated with early T cell progenitors (Lee et al., 2004), and undifferentiated tumors (Rhodes et al., 2004) were also enriched. *Fbxw7*, on the other hand, was significantly downregulated in the Myc<sup>GFP+</sup> population (Figure 3F), suggesting that, in the absence of mutations, there is a need to transcriptionally downregulate its activity during leukemic progression (Mavrakis et al., 2011).

### Myc Deletion Specifically Targets LICs in an Animal Model of T-ALL

Given that leukemia-initiating capacity was found to be restricted to the Myc<sup>GFP+</sup> population, we tested whether the depletion of *Myc* could specifically ablate LIC activity in T-ALL. Primary T-ALLs were generated from *Myc<sup>F/F</sup>Mx1-Cre<sup>+</sup>* or *Myc<sup>+/-</sup>Mx1-Cre<sup>+</sup>* donors, and recipients were injected with pI:pC 2 weeks later, after leukemic cells were detected in the periphery. Our initial observation was that leukemic burden was decreased in recipients in which c-Myc expression was deleted (Figure 4A). Strikingly, the LIC-enriched DN3 subset was almost completely absent in the *Myc*-deficient leukemias (Figure 4B), suggesting that the LIC population absolutely depends on c-Myc function in vivo. To test this hypothesis further, we trans-

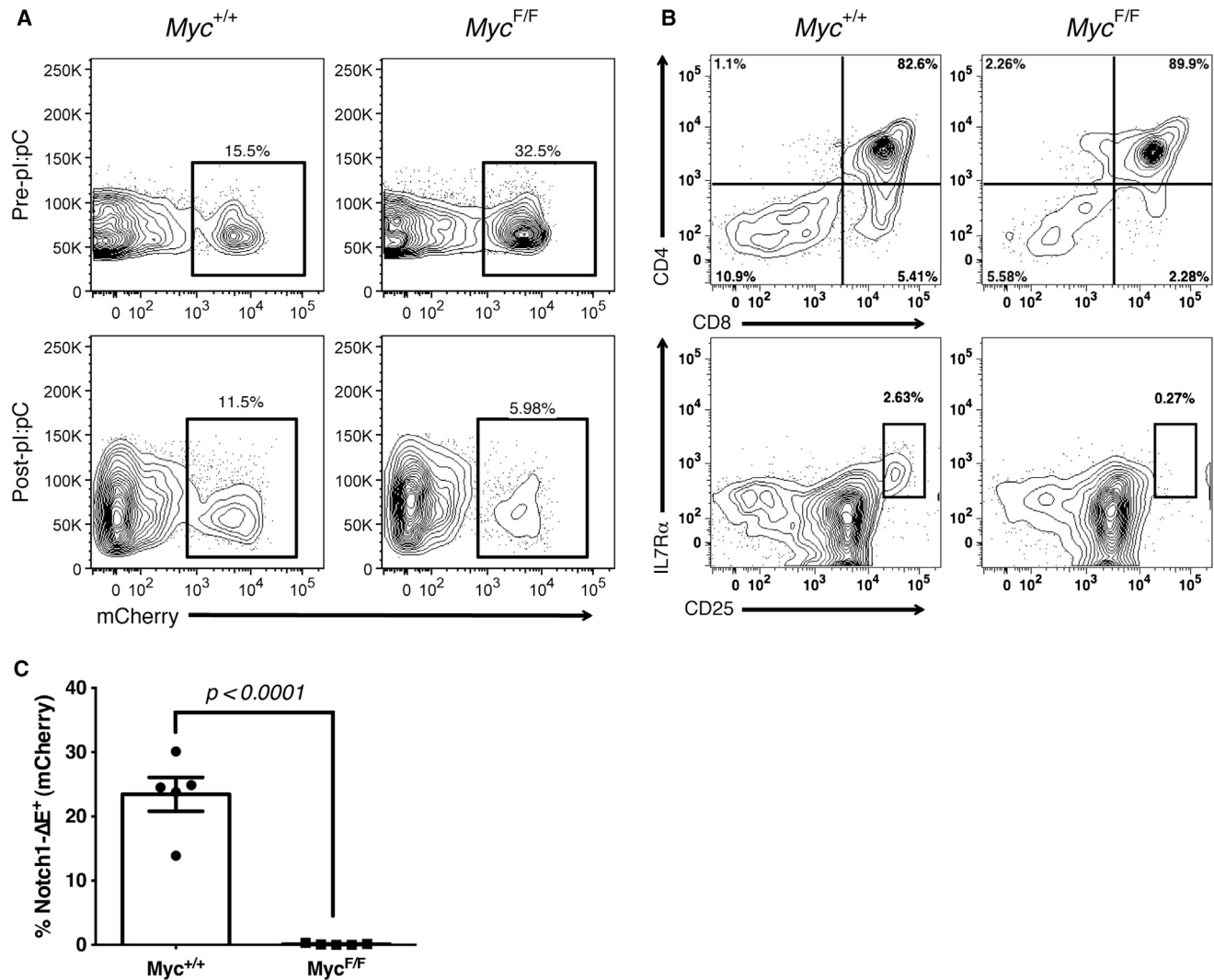
planted equal numbers of Notch1ΔE<sup>+</sup> cells from either the pl-pC-treated *Myc<sup>F/F</sup>* or *Myc<sup>+/-</sup>* primary T-ALL and assessed leukemia development in secondary hosts. We found that, although the *Myc* WT cells effectively generated secondary tumors, no leukemic cells were detected in the *Myc*-deficient group (Figure 4C), demonstrating the absence of functional LICs.

### BET Inhibitors Efficiently Suppress Growth of Mouse and Human T-ALL

Recently, selective BET bromodomain inhibitors were identified to specifically target BRD4, a transcriptional activator of MYC (Delmore et al., 2011; Devaiah et al., 2012; Filippakopoulos et al., 2010; Mertz et al., 2011; Zuber et al., 2011). One of these molecules, JQ1, was shown to effectively inhibit the expression and function of MYC, and it inhibited cell growth in multiple myeloma and acute myeloid leukemia (Filippakopoulos et al., 2010; Mertz et al., 2011). To determine whether the inhibition of BRD4 could similarly lead to growth inhibition in T-ALL, we initially compared retroviral shRNA knockdown of *Myc* and *Brd4* in Notch1<sup>+</sup> mouse T-ALL cell lines. A significant loss of representation over time was observed in populations expressing shRNA targeting either gene (Figure S5A). The growth effect induced by the MYC hairpins was on target, given that complementation with non-RNA interference (RNAi)-targeted MYC cDNA restored their growth potential (Figure S5B).

To start addressing the putative leukemia-targeting properties of BET inhibitors, we tested the growth of human T-ALL lines in the presence of varying concentrations of JQ-1 in vitro (Figure 5A). A significant decrease in cell growth was observed after 4 days of JQ-1 treatment in a dose-dependent manner. BrdU incorporation assays and AnnexinV staining suggested that JQ-1 treatment resulted primarily in growth arrest rather than apoptosis (Figures 5B–5C). Given that previous work has shown that FBXW7 mutations conferred resistance to gamma-secretase inhibitors (GSIs) (Real et al., 2009; Thompson et al., 2007), response to JQ-1 or GSI (Compound E) was compared in FBXW7 mutant or WT T-ALL lines (Figure 5D). As expected, GSI treatment inhibited the growth of HPB-ALL cells (WT FBXW7) but was significantly less effective in CEM or Jurkat T cells (both FBXW7 mutants). However, all T-ALL lines were unable to grow in the presence of JQ-1. The observed growth arrest was due, at least in part, to a loss of c-Myc, given that JQ-1 treatment resulted in a significant reduction in c-Myc protein expression in all T-ALL lines tested (Figure 5E) and overexpression of c-Myc partially restored proliferation of the treated cells (Figure 5F). Altogether, these results show that BET bromodomain inhibitors are an appealing alternative to GSI treatment because they are able to target T-ALL cells irrespective of FBXW7 mutations.

In order to determine the in vivo efficacy of BET inhibitors with mouse T-ALL models, it was necessary to establish an in vitro system to maintain and expand c-Myc<sup>GFP+</sup> LICs. Primary Notch1ΔE<sup>+</sup>c-Myc<sup>GFP+</sup> splenocytes lose expression of c-Myc<sup>GFP</sup> and fail to expand in liquid culture (Figure S5C). However, when cocultured on OP9 stromal line in the presence of IL-7, these cells maintain their expression of c-Myc<sup>GFP</sup> (Figure S5C) and can be expanded indefinitely. Upon treatment with JQ-1, expression of c-Myc<sup>GFP</sup> rapidly returns to basal levels (Figure 6A)



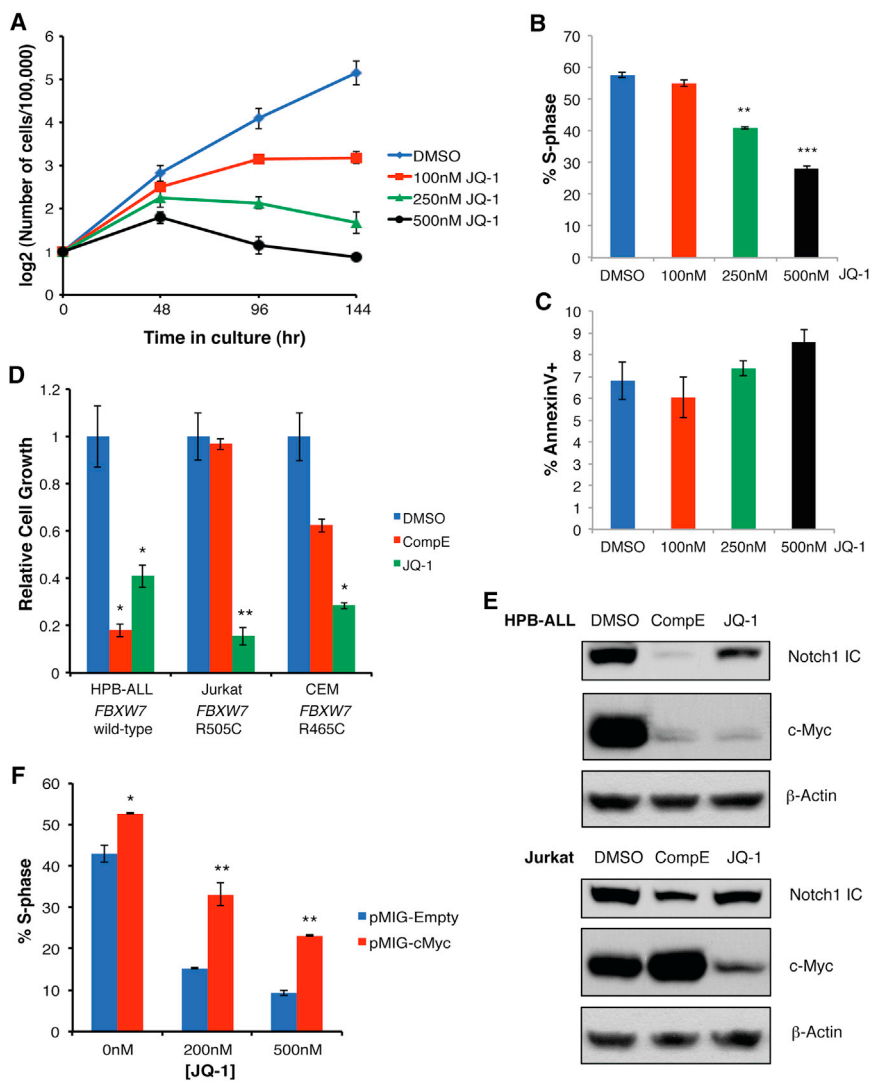
**Figure 4. Genetic Depletion of *Myc* Expression Abolishes Leukemia-Initiating Activity in T-ALL**

(A) *Myc*<sup>+/+</sup>*Mx1Cre*<sup>+</sup> or *Myc*<sup>F/F</sup>*Mx1Cre*<sup>+</sup> BM was transduced with Notch1 $\Delta E$  and transplanted into lethally irradiated recipients. Notch1 $\Delta E^+$  T-ALL cells were measured in peripheral blood 2 weeks after transplant (top) and 7 days after pl:pC treatment (bottom). (B) FACS analysis showing the frequency of Notch1 $\Delta E^+$  cells expressing CD4 and CD8 (top) and CD4<sup>-</sup>CD8<sup>-</sup>CD25<sup>hi</sup>IL-7R $\alpha^+$  (bottom) immunophenotype within spleen following Cre induction. (C) Frequency of Notch1 $\Delta E^+$  PBMC in secondary recipients of *Myc* WT and deficient T-ALL cells 2 weeks after transplant. Error bars indicate mean  $\pm$  SD. See also Figure S5.

and the growth of the T-ALL cells is significantly inhibited (Figure 6B). To study the effect of BET bromodomain inhibitors on the progression of T-ALL in vivo, we utilized a derivative of JQ1, CPI203 (Devaiah et al., 2012), which has shown superior bioavailability with oral or intraperitoneal (i.p.) administration. The EC<sub>50</sub> of CPI203 was nearly 3-fold lower than JQ-1 (91.2 versus 263 nM) when tested on a primary mouse T-ALL in vitro (Figure 6B), and this corresponded to a decrease in *Myc* mRNA (Figure 6C). To measure the effect of CPI203 in vivo, two independently derived primary mouse T-ALL samples, either *Fbxw7*<sup>+/+</sup> or *Fbxw7*<sup>mut/+</sup>, were transduced with a lentiviral luciferase reporter and each transplanted into two recipient animal groups, one treated with CPI203 (5 mg kg<sup>-1</sup>, BID) and the other

with vehicle, and disease progression was monitored by in vivo luciferase imaging (IVIS Lumina) (Figure 6D). A significant and rapid reduction in leukemia burden was observed in both the recipient groups treated with CPI203 (Figures 6D–6E), thus demonstrating the therapeutic potential of this compound for use in vivo.

Finally, we tested the response of primary human T-ALL patient samples (all with activating *NOTCH1* mutations  $\pm$  *FBXW7* missense mutations) to both JQ1 and CPI203. Typically, a 2- to 3-fold reduction in cell growth occurred upon treatment with either compound across all genotypes (Figure S6A). Similarly to what was observed in the cell lines, this effect could be attributed mainly to cell-cycle arrest (Figure S6B), although a modest



**Figure 5. BET Bromodomain Inhibition Broadly Impacts the Growth of Human T-ALL**

(A–C) A dose response curve showing the growth of a CUTLL1 human T-ALL line (*FBXW7* WT) treated with increasing concentrations of JQ-1 or vehicle. The frequency of cells that incorporated BrdU during a 1 hr pulse (B) or stained positive for Annexin V (C) was determined after treatment with JQ-1 for 48 hr.

(D) Growth of human T-ALL lines treated with GSI (Compound E) or JQ-1 in vitro after 4 days relative to vehicle-treated controls.

(E) Immunoblot for Notch1 ICD and c-Myc in T-ALL lines treated with inhibitors.

(F) We treated 720 cells transduced with pMIG, either empty or bearing a c-Myc cDNA, for 72 hr with JQ-1 at the indicated concentration and pulsed them with BrdU for 1 hr, and the frequency of GFP<sup>+</sup> cells in S phase was determined by flow cytometry. Error bars indicate mean ± SD. \*p < 0.05; \*\*p < 0.01; \*\*\*p < 0.001.

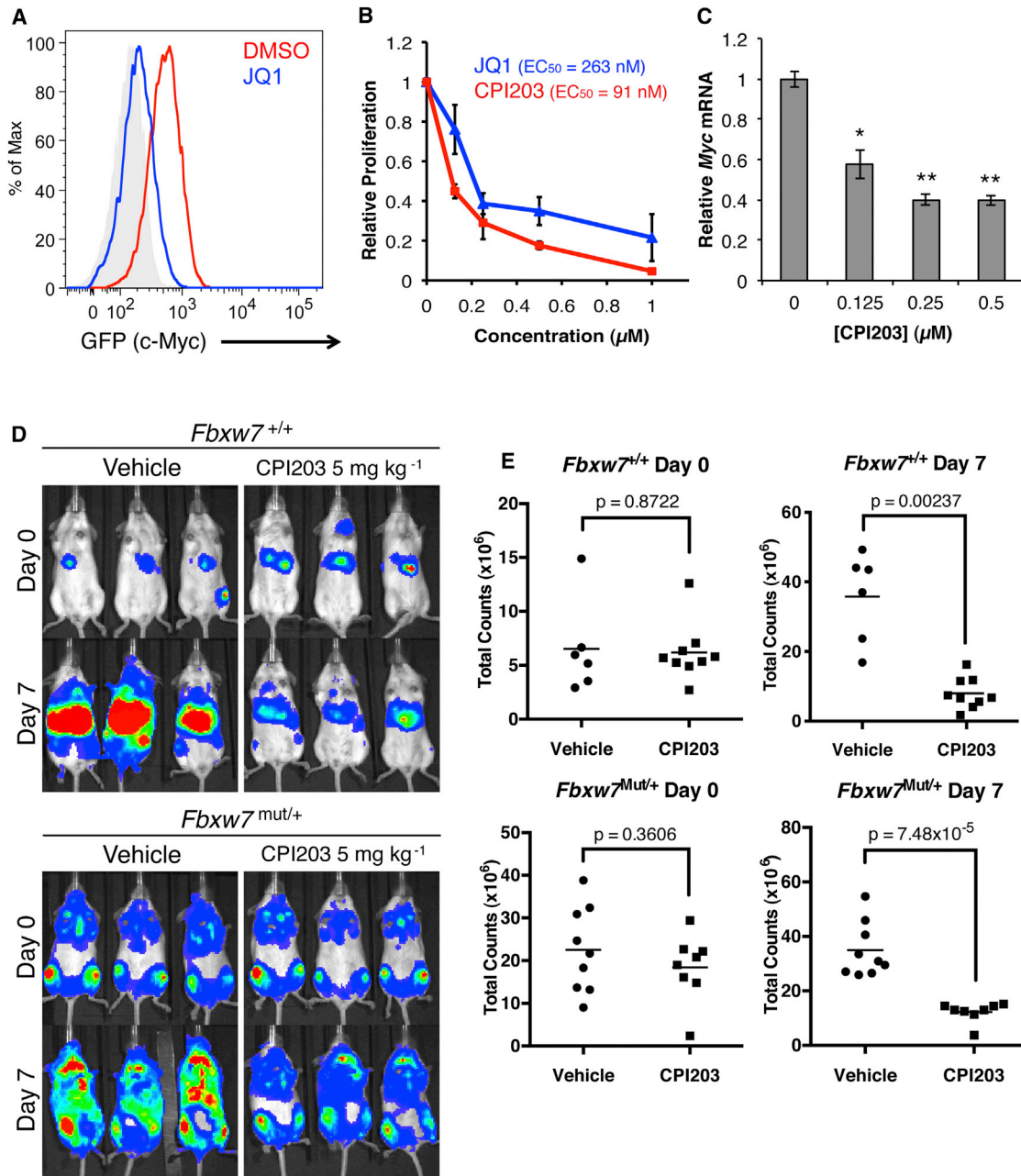
See also Figure S6.

T-ALL model (Figure 3F). High-throughput chromatin immunoprecipitation sequencing (ChIP-seq) for c-Myc and Brd4 was performed in CUTLL1 cells to assess their genome-wide occupancy. A total of 6,335 genes had significant c-Myc binding, and 6,874 genes showed significant Brd4 occupancy. Using available Notch1 and Rbpj ChIP-seq data (Wang et al., 2012), we compared the 7,526 genes also bound by both of these factors. A significant fraction of all occupied genes (3,282 of 9,453) showed binding for all three of these factors, suggesting an overlapping regulatory network (Figure 7B). As expected, a large portion of

genes that were downregulated upon JQ-1 treatment also showed high promoter-read density for Brd4, c-Myc, or Notch1 (Figure 7C). Accordingly, a specific loss of Brd4 binding is observed at target gene promoters and enhancers (Figure S7), and this loss is to a greater extent than Brd2, demonstrating some specificity of BET inhibition. In order to investigate the impact of c-Myc and Brd4 binding on direct targets of Notch and Rbpj, we categorized expressed genes (FPKM > 5) on the basis of the presence of all three factors, c-Myc, Notch1 only, or Notch1 alone. We found that genes with Brd4, c-Myc, and Notch1 binding have significantly higher expression than those with Notch binding alone. Genes with Brd4, c-Myc, and Notch1 binding or c-Myc and Notch1 binding also showed significantly higher RNA PolII density at their promoters, implying that the presence of c-Myc and Brd4, in addition to Notch1 at promoters, enhances transcriptional activity. Altogether, these data suggest that, especially in the context of *FBXW7* mutations, higher thresholds of c-Myc work together with Notch1 activation to amplify a subset of genes critical for leukemic transformation.

**BET Inhibitors Target the Notch and Myc Oncogenic Transcriptional Program**

Brd4 functions as a chromatin reader by binding acetylated histones and recruiting effectors of transcriptional elongation, thereby promoting gene activation (Hargreaves et al., 2009). Thus, we hypothesized that Brd4 inhibition might have profound effects on T-ALL gene expression. High-throughput RNA sequencing (RNA-seq) was performed in CUTLL1 cells after treatment with inhibitor to assess immediate consequences on transcription genome wide. A total of 1,696 genes were downregulated, and 1,287 genes were upregulated upon JQ-1 treatment for 12 hr (400 nM) in comparison to vehicle-treated control (Max FPKM > 5, fold change > 1.3, q < 0.05) (Figure 7A). Interestingly, 28% of genes downregulated upon JQ-1 treatment were also overexpressed in the Myc<sup>GFP+</sup> LIC population in our mouse



**Figure 6. BET Bromodomain Inhibitors Deplete LICs and Inhibit the Progression of T-ALL Both In Vitro and In Vivo**

(A) A histogram depicting c-Myc<sup>GFP</sup> levels in primary Notch1ΔE ires mCherry<sup>+</sup>c-Myc<sup>GFP</sup> splenocytes cocultured on OP9 stromal cells in the presence of 5 ng/ml IL-7 and either 200 nM JQ-1 or DMSO.

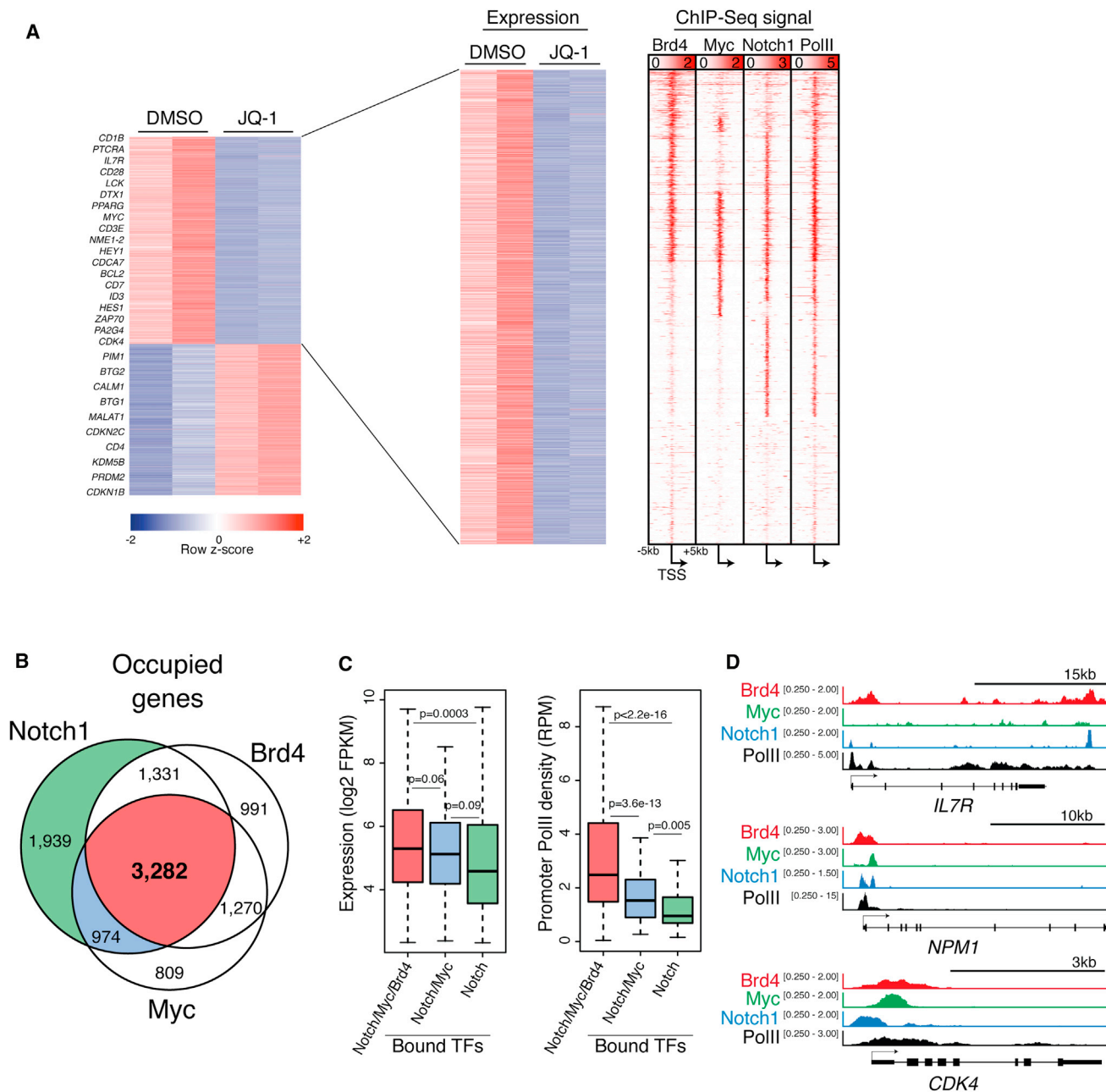
(B) Growth of primary mouse T-ALL treated with increasing concentrations of JQ-1 or CPI203 for 72 hr. Calculated EC<sub>50</sub> for each compound is shown.

(C) Myc mRNA measured by qRT-PCR in primary mouse T-ALL cells treated with CPI203 for 4 hr at the indicated concentration.

(D) Bioluminescent imaging of recipient mice transplanted either *Fbxw7*<sup>+/+</sup> (top) or *Fbxw7*<sup>mut/+</sup> (bottom) Notch1ΔE leukemias and treated with either CPI203 (5 mg kg<sup>-1</sup>) or vehicle BID for 7 days. Quantification of total bioluminescent counts, each data point representing an individual mouse, before and following 7 days of the indicated treatment.

Error bars for (B) and (C) indicate mean ± SD for three biological replicates. \*p < 0.05; \*\*p < 0.01.

See also Figures S5 and S6.



**Figure 7. BRD4 Inhibition Reduces the Expression of Genes Directly Regulated by MYC and NOTCH1**

(A) Heat maps showing genes significantly downregulated upon treatment of CUTLL1 cells with JQ-1 (400 nM) for 12 hr in comparison to vehicle treated as determined by high-throughput RNA-seq. Each column represents a biological replicate. ChIP-seq signal density heat maps (right) show Brd4, c-Myc, Notch1, and total RNA PolII at gene loci depicted in the gene expression heatmap. Genes are clustered based on Brd4, c-Myc, and Notch1 signal density. Scale represents reads per million (RPM). (B) A Venn diagram showing the overlap of total genes bound by Brd4, c-Myc, and Notch1 in CUTLL1 cells. (C) Box plots showing Log2FPKM values (left) or promoter PolII density (right) for genes bound by combinations of Brd4, c-Myc, and Notch. Whiskers represent the upper and lower limits of the range. Boxes represent the first and third quartile, and the line represents the median. (D) Representative ChIP-seq tracks for three gene loci: *IL7R*, *NPM1*, and *CDK4*. The scale corresponds to RPM. See also Figure S7.

## DISCUSSION

The presented study sheds light on the selection of *FBXW7* mutations during the evolution of leukemia genomes and the sig-

nificant bias for missense (but fewer nonsense, insertion, or deletion) mutations in human T-ALL. The differential function of *FBXW7* mutations could be explained by the existence of distinct thresholds of c-Myc expression between normal and malignant

stem cells. This observation reveals a potential therapeutic window for the modulation of Fbxw7 and Myc activity in the treatment of human cancers. Indeed, we were able to show that *Myc* deletion suppresses established T-ALL by eliminating LICs and that pharmacologic targeting of c-Myc induction restricted the growth of human and mouse T-ALL, including those that carry *FBXW7* mutations and are resistant to Notch inhibition.

Another important finding illustrated here is that we are able to visualize LICs using in vivo genetic fluorescent labeling. Using the c-Myc<sup>GFP</sup> reporter strain, we were able to demonstrate that LICs can be purified on the basis of c-Myc protein abundance. T-ALL LICs have a characteristic surface phenotype, and their gene expression patterns correlate to gene signatures characteristic of earlier stages of differentiation, including HSCs and ESCs. Interestingly, a large proportion of these LIC-specific genes are bound by c-Myc and Notch1, both of which are key oncogenes in T-ALL. Brd4 is also present at most of these loci, a finding that can explain the therapeutic efficacy of BET inhibitors. Moreover, we observed that c-Myc expression directly correlated to LIC populations in vivo. Accordingly, human T-ALL LIC-enriched populations also express high levels of c-Myc protein, and *FBXW7* mutations lead to significant c-Myc stabilization, suggesting that this mechanism is evolutionarily conserved. However, this is not a universal characteristic of tumor-initiating cell populations. Indeed, we have recently performed studies using animal models of BCR-ABL-driven chronic myelogenous leukemia, a prototypic LIC-driven disease. In this leukemia model, c-Myc expression does not define the cell population that has the ability to initiate and propagate disease (Reavie et al., 2013), suggesting that different oncogenes and cellular settings could have distinct requirements for c-Myc expression and function.

Although c-Myc is critical in the development of a wide range of tissues, recent studies have suggested that c-Myc inhibition is surprisingly well tolerated, at least in preclinical animal studies (Soucek et al., 2008). Initially, the inhibition of the Notch pathway with GSIs was a promising therapeutic approach, but it has presented considerable challenges (gastrointestinal toxicity and acquisition of resistance, for example) for its adaptation in the clinic. Here, we show that genetic inactivation of *Myc* in established T-ALL specifically targeted the LIC fraction, eventually leading to tumor regression and loss of LIC self-renewal. Similarly, treatment of human T-ALL lines and primary leukemic cells with BET inhibitors (JQ1 and CPI203) completely suppressed c-Myc response, leading to rapid growth arrest. Unlike GSI treatment, this effect is irrespective of *FBXW7* status, suggesting such compounds could have broader applications across tumor genotypes. It remains to be seen whether BET inhibition will be as efficient for the treatment of either relapsed T-ALL or highly aggressive T-ALL subtypes, including early T cell progenitor T-ALL, which is also resistant to Notch pathway inhibition (Zhang et al., 2012).

The combination of disease modeling to whole-genome and transcriptome studies lead to findings that could have major implications for the understanding of oncogenic (Notch and Myc) interactions and their role in gene expression regulation and cancer initiation. Our studies show that Notch1 is not sufficient to

induce or maintain transplantable T-ALL in the absence of c-Myc. Interestingly, we demonstrate that the majority of LIC-specific genes are bound by both transcription factors, but deletion of *Myc* can abrogate LIC activity. In agreement to this notion, it has been shown in vitro that *MYC* overexpression can induce resistance to Notch pathway inhibition (Weng et al., 2006). Thus, we hypothesize that Notch1 acts as a pioneering factor, influencing lineage commitment and the activity of epigenetic regulators (Ntziachristos et al., 2012), altering the chromatin structure of its transcriptional targets to a more permissive state. When c-Myc becomes expressed and stabilized (because of the mutation or downregulation of *FBXW7*), it can bind to newly accessible E box motifs, thereby amplifying established gene-expression programs (Figure 7C). These studies support, in an in vivo tumor model, the recently postulated “MYC transcriptional amplification” hypothesis (Lin et al., 2012; Nie et al., 2012). They also prove that this transcriptional amplification mode has in vivo consequences in cancer initiation and can be pharmacologically targeted. Finally, our studies show that such key transcriptional responses can be posttranslationally regulated and that oncogenic events invent ways to hijack them, as shown with in vivo modeling of the *FBXW7* missense mutations.

## EXPERIMENTAL PROCEDURES

### Mice

c-Myc GFP knockin and *Myc* conditional knockout mice were as described previously (de Alboran et al., 2001; Huang et al., 2008). *Fbxw7* knockin mutant mice were generated by the insertion of a loxP-flanked splice acceptor PGK-NEO cassette with three polyA sites in the intronic sequence between exons 10 and 11, and a CCG-to-GCA point mutation was introduced by PCR mutagenesis in the opposite strand at a coding sequence corresponding to R468. *Eef1a1* human *FBXW7*<sup>R465C</sup> mice were generated by introducing an R465C mutation into an N-terminally FLAG M2-tagged human *FBXW7* alpha cDNA and subcloning this sequence into an *Eef1a1* lox-STOP-lox targeting vector, as described previously (Buonamici et al., 2009). Inducible Cre recombinase expression was achieved in Mx1-Cre mice by three consecutive i.p. injections of poly(I):poly(C) (15 mg kg<sup>-1</sup>, GE Healthcare). CPI203 (Constellation Pharmaceuticals) was dissolved in 5% DMSO and 10% hydroxypropyl-beta cyclodextrin and administered by i.p. injection twice daily at 5 mg kg<sup>-1</sup>. All animal experiments were done in accordance with the guidelines of the NYU School of Medicine or the Columbia University Institutional Animal Care and Use Committee.

### Bone Marrow Transduction and Transplantation

BM was enriched for hematopoietic stem and progenitor cells by the magnetic selection of cells expressing c-kit (STEMCELL Technologies) cultured in the presence of 50 ng/ml SCF, 50 ng/ml Flt3 ligand, 10 ng/ml IL-3, and 10 ng/ml IL-6 and infected with concentrated retroviral supernatants after 24 and 48 hr. Transduction efficiency was determined by reporter fluorescence at 96 hr, and total or sorted populations were transferred via retroorbital injection into irradiated (1,100 rad) congenic recipients along with 2 × 10<sup>5</sup> unfractionated bone marrow mononuclear cells (BMMCs) for hemogenic support. Sublethally irradiated (450 rad) mice were used for secondary transplants. For Notch1 T-ALL induction, 5 × 10<sup>4</sup> Notch1ΔE GFP<sup>+</sup> BM cells were transferred per recipient, unless otherwise stated.

### In Vitro Drug Treatments

Human and mouse T-ALL lines were grown in complete RPMI media (supplemented with 10% fetal bovine serum, penicillin and streptomycin, glutamine, and 55 μM β-mercaptoethanol). Primary mouse T-ALL were cocultured with OP9 stromal cells in Opti-MEM supplemented with 10% fetal bovine serum, 5 ng/ml IL-7, penicillin and streptomycin, glutamine, and 55 μM β-mercaptoethanol and passaged every 3–4 days onto a fresh feeder layer. JQ1



(Cayman Chemical) or Compound E (Alexis Biochemicals) prepared in DMSO was added to the cultures, and the media was replaced every 24 hr. BrdU (10  $\mu$ M) was added for a 1 hr pulse, and incorporation into DNA was determined by using the BrdU Flow Kit (BD Pharmingen).

### Chromatin Immunoprecipitation

ChIP-seq was performed in CUTLL1 cells with rabbit polyclonal antibodies against c-Myc (N-262, Santa Cruz Biotechnology), Brd2 (Bethyl Laboratories, A302-583A), or Brd4 (Bethyl Laboratories, A301-985A) (5  $\mu$ g per i.p. injection) as described previously (Ntziachristos et al., 2012). Peak calling was performed with MACS1.4, allowing only one duplicate read. For Notch1, we considered only peaks with  $p < 10 \times 10^{-7}$ . For c-Myc and Brd4, we considered peaks with  $p < 10 \times 10^{-5}$ . Peak annotation was performed with a Cis-regulatory element annotation system. Genes were considered bound if a peak was present within 2 kb of the transcription start site.

### Statistical Analysis

The means of each data set were analyzed using a Student's *t* test with a two-tailed distribution and assuming equal sample variance.

### ACCESSION NUMBERS

Raw expression data were deposited in the Gene Expression Omnibus under accession number GSE46797.

### SUPPLEMENTAL INFORMATION

Supplemental Information includes Extended Experimental Procedures and seven figures and can be found with this article online at <http://dx.doi.org/10.1016/j.cell.2013.05.041>.

### ACKNOWLEDGMENTS

We thank Constellation Pharmaceuticals for providing CPI203; W. Pear, P. Premisriut, J. Aster, J. Silva, M. Kelliher, and A. Klinakis for sharing materials; J. Zavadil and the NYU Genome Technology Center (supported in part by an NIH/NCI P30 CA016087-30 grant) for assistance with microarrays; L. Deriano and J. Chaumeil for mFISH analysis; the NYU Flow Cytometry facility for cell sorting; and the NYU Histology Core and Transgenic Mouse Core (NYU Cancer Institute Center grant 5P30CA16087-31). I.A. was supported by the NIH (1RO1CA133379, 1RO1CA105129, 1RO1CA149655, 5RO1CA173636, and 1RO1GM088847). I.A. was also supported by the William Lawrence and Blanche Hughes Foundation, the Leukemia & Lymphoma Society (TRP#6340-11 and LLS#6373-13), the Chemotherapy Foundation, the Irma T. Hirsch Trust, the V Foundation for Cancer Research, the St. Baldrick's Foundation, and a Feinberg Lymphoma Grant. B.K. was supported by the NYU CMB Training Program. L.R. is supported by a Ruth L. Kirschstein F31 Award and a Marie Curie Actions Fellowship. J.M. is supported by NWO Rubicon and the Dutch Cancer Society. I.A. is a Howard Hughes Medical Institute Early Career Scientist. I.A. and B.K. designed experiments and wrote the manuscript. B.K. performed most of the experiments. L.R. generated Eef1a1-targeted ESCs. L.X., A.P.-G., and A.F. assisted with in vivo and primary human T-ALL drug studies. P.S. assisted with inhibitor production and provided advice for use. C.V., J.S., and J.M. performed BRD4 knockdown experiments. B.A.-O. performed ubiquitylation assays. P.N., T.T., and S.S.S. performed and analyzed RNA-seq and ChIP-seq experiments. P.S. is an employee of Constellation Pharmaceuticals.

Received: October 13, 2012

Revised: March 26, 2013

Accepted: May 21, 2013

Published: June 20, 2013

### REFERENCES

Aifantis, I., Raetz, E., and Buonamici, S. (2008). Molecular pathogenesis of T-cell leukaemia and lymphoma. *Nat. Rev. Immunol.* 8, 380–390.

Akhoondi, S., Sun, D., von der Lehr, N., Apostolidou, S., Klotz, K., Maljukova, A., Cepeda, D., Fiegl, H., Dafou, D., Marth, C., et al. (2007). FBXW7/hCDC4 is a general tumor suppressor in human cancer. *Cancer Res.* 67, 9006–9012.

Armstrong, F., Brunet de la Grange, P., Gerby, B., Rouyez, M.C., Calvo, J., Fontenay, M., Boissel, N., Dombret, H., Baruchel, A., Landman-Parker, J., et al. (2009). NOTCH is a key regulator of human T-cell acute leukemia initiating cell activity. *Blood* 113, 1730–1740.

Aster, J.C., Robertson, E.S., Hasserjian, R.P., Turner, J.R., Kieff, E., and Sklar, J. (1997). Oncogenic forms of NOTCH1 lacking either the primary binding site for RBP-Jkappa or nuclear localization sequences retain the ability to associate with RBP-Jkappa and activate transcription. *J. Biol. Chem.* 272, 11336–11343.

Buchstaller, J., McKeever, P.E., and Morrison, S.J. (2012). Tumorigenic cells are common in mouse MPNSTs but their frequency depends upon tumor genotype and assay conditions. *Cancer Cell* 21, 240–252.

Buonamici, S., Trimarchi, T., Ruocco, M.G., Reavie, L., Cathelin, S., Mar, B.G., Klinakis, A., Lukyanov, Y., Tseng, J.C., Sen, F., et al. (2009). CCR7 signalling as an essential regulator of CNS infiltration in T-cell leukaemia. *Nature* 459, 1000–1004.

Chiang, M.Y., Xu, L., Shestova, O., Histen, G., L'heureux, S., Romany, C., Childs, M.E., Gimotty, P.A., Aster, J.C., and Pear, W.S. (2008). Leukemia-associated NOTCH1 alleles are weak tumor initiators but accelerate K-ras-initiated leukemia. *J. Clin. Invest.* 118, 3181–3194.

Crusio, K.M., King, B., Reavie, L.B., and Aifantis, I. (2010). The ubiquitous nature of cancer: the role of the SCF(Fbw7) complex in development and transformation. *Oncogene* 29, 4865–4873.

Davis, H., Lewis, A., Spencer-Dene, B., Tateossian, H., Stamp, G., Behrens, A., and Tomlinson, I. (2011). FBXW7 mutations typically found in human cancers are distinct from null alleles and disrupt lung development. *J. Pathol.* 224, 180–189.

de Alboran, I.M., O'Hagan, R.C., Gärtner, F., Malyln, B., Davidson, L., Rickert, R., Rajewsky, K., DePinho, R.A., and Alt, F.W. (2001). Analysis of C-MYC function in normal cells via conditional gene-targeted mutation. *Immunity* 14, 45–55.

Delmore, J.E., Issa, G.C., Lemieux, M.E., Rahl, P.B., Shi, J., Jacobs, H.M., Kastriitis, E., Gilpatrick, T., Paranal, R.M., Qi, J., et al. (2011). BET bromodomain inhibition as a therapeutic strategy to target c-Myc. *Cell* 146, 904–917.

Devaiah, B.N., Lewis, B.A., Cherman, N., Hewitt, M.C., Albrecht, B.K., Robey, P.G., Ozato, K., Sims, R.J., 3rd, and Singer, D.S. (2012). BRD4 is an atypical kinase that phosphorylates serine2 of the RNA polymerase II carboxy-terminal domain. *Proc. Natl. Acad. Sci. USA* 109, 6927–6932.

Downing, J.R., Wilson, R.K., Zhang, J., Mardis, E.R., Pui, C.H., Ding, L., Ley, T.J., and Evans, W.E. (2012). The Pediatric Cancer Genome Project. *Nat. Genet.* 44, 619–622.

Eilers, M., and Eisenman, R.N. (2008). Myc's broad reach. *Genes Dev.* 22, 2755–2766.

Ferrando, A.A., and Look, A.T. (2003). Gene expression profiling in T-cell acute lymphoblastic leukemia. *Semin. Hematol.* 40, 274–280.

Filippakopoulos, P., Qi, J., Picaud, S., Shen, Y., Smith, W.B., Fedorov, O., Morse, E.M., Keates, T., Hickman, T.T., Felletar, I., et al. (2010). Selective inhibition of BET bromodomains. *Nature* 468, 1067–1073.

Francis, R., and Richardson, C. (2007). Multipotent hematopoietic cells susceptible to alternative double-strand break repair pathways that promote genome rearrangements. *Genes Dev.* 21, 1064–1074.

Grabher, C., von Boehmer, H., and Look, A.T. (2006). Notch 1 activation in the molecular pathogenesis of T-cell acute lymphoblastic leukaemia. *Nat. Rev. Cancer* 6, 347–359.

Grim, J.E., Knoblaugh, S.E., Guthrie, K.A., Hagar, A., Swanger, J., Hespelt, J., Delrow, J.J., Small, T., Grady, W.M., Nakayama, K.I., and Clurman, B.E. (2012). Fbw7 and p53 cooperatively suppress advanced and chromosomally unstable intestinal cancer. *Mol. Cell. Biol.* 32, 2160–2167.

- Hargreaves, D.C., Hornig, T., and Medzhitov, R. (2009). Control of inducible gene expression by signal-dependent transcriptional elongation. *Cell* 138, 129–145.
- Hodis, E., Watson, I.R., Kryukov, G.V., Arold, S.T., Imielinski, M., Theurillat, J.P., Nickerson, E., Auclair, D., Li, L., Place, C., et al. (2012). A landscape of driver mutations in melanoma. *Cell* 150, 251–263.
- Huang, C.Y., Bredemeyer, A.L., Walker, L.M., Bassing, C.H., and Sleckman, B.P. (2008). Dynamic regulation of c-Myc proto-oncogene expression during lymphocyte development revealed by a GFP-c-Myc knock-in mouse. *Eur. J. Immunol.* 38, 342–349.
- Kim, J., Chu, J., Shen, X., Wang, J., and Orkin, S.H. (2008). An extended transcriptional network for pluripotency of embryonic stem cells. *Cell* 132, 1049–1061.
- Klinakis, A., Szabolcs, M., Chen, G., Xuan, S., Hibshoosh, H., and Efstratiadis, A. (2009). Igf1r as a therapeutic target in a mouse model of basal-like breast cancer. *Proc. Natl. Acad. Sci. USA* 106, 2359–2364.
- Kühn, R., Schwenk, F., Aguet, M., and Rajewsky, K. (1995). Inducible gene targeting in mice. *Science* 269, 1427–1429.
- Lee, M.S., Hanspers, K., Barker, C.S., Korn, A.P., and McCune, J.M. (2004). Gene expression profiles during human CD4+ T cell differentiation. *Int. Immunol.* 16, 1109–1124.
- Lin, C.Y., Lovén, J., Rahl, P.B., Paranal, R.M., Burge, C.B., Bradner, J.E., Lee, T.I., and Young, R.A. (2012). Transcriptional amplification in tumor cells with elevated c-Myc. *Cell* 151, 56–67.
- Margolin, A.A., Palomero, T., Sumazin, P., Califano, A., Ferrando, A.A., and Stolovitzky, G. (2009). ChIP-on-chip significance analysis reveals large-scale binding and regulation by human transcription factor oncogenes. *Proc. Natl. Acad. Sci. USA* 106, 244–249.
- Matsuoka, S., Oike, Y., Onoyama, I., Iwama, A., Arai, F., Takubo, K., Mashimo, Y., Oguro, H., Nitta, E., Ito, K., et al. (2008). Fbxw7 acts as a critical fail-safe against premature loss of hematopoietic stem cells and development of T-ALL. *Genes Dev.* 22, 986–991.
- Mavrakis, K.J., Van Der Meulen, J., Wolfe, A.L., Liu, X., Mets, E., Taghon, T., Khan, A.A., Setty, M., Rondou, P., Vandenberghe, P., et al. (2011). A cooperative microRNA-tumor suppressor gene network in acute T-cell lymphoblastic leukemia (T-ALL). *Nat. Genet.* 43, 673–678.
- Mertz, J.A., Conery, A.R., Bryant, B.M., Sandy, P., Balasubramanian, S., Mele, D.A., Bergeron, L., and Sims, R.J., 3rd. (2011). Targeting MYC dependence in cancer by inhibiting BET bromodomains. *Proc. Natl. Acad. Sci. USA* 108, 16669–16674.
- Mohrin, M., Bourke, E., Alexander, D., Warr, M.R., Barry-Holson, K., Le Beau, M.M., Morrison, C.G., and Passegué, E. (2010). Hematopoietic stem cell quiescence promotes error-prone DNA repair and mutagenesis. *Cell Stem Cell* 7, 174–185.
- Murphy, M.J., Wilson, A., and Trumpp, A. (2005). More than just proliferation: Myc function in stem cells. *Trends Cell Biol.* 15, 128–137.
- Nash, P., Tang, X., Orlicky, S., Chen, Q., Gertler, F.B., Mendenhall, M.D., Sicheri, F., Pawson, T., and Tyers, M. (2001). Multisite phosphorylation of a CDK inhibitor sets a threshold for the onset of DNA replication. *Nature* 414, 514–521.
- Nie, Z., Hu, G., Wei, G., Cui, K., Yamane, A., Resch, W., Wang, R., Green, D.R., Tessarollo, L., Casellas, R., et al. (2012). c-Myc is a universal amplifier of expressed genes in lymphocytes and embryonic stem cells. *Cell* 151, 68–79.
- Ntziachristos, P., Tsirigos, A., Van Vlierberghe, P., Nedjic, J., Trimarchi, T., Flaherty, M.S., Ferres-Marco, D., da Ros, V., Tang, Z., Siegle, J., et al. (2012). Genetic inactivation of the polycomb repressive complex 2 in T cell acute lymphoblastic leukemia. *Nat. Med.* 18, 298–301.
- O’Neil, J., Grim, J., Strack, P., Rao, S., Tibbitts, D., Winter, C., Hardwick, J., Welcker, M., Meijerink, J.P., Pieters, R., et al. (2007). FBW7 mutations in leukemia cells mediate NOTCH pathway activation and resistance to gamma-secretase inhibitors. *J. Exp. Med.* 204, 1813–1824.
- Onoyama, I., Tsunematsu, R., Matsumoto, A., Kimura, T., de Alborán, I.M., Nakayama, K., and Nakayama, K.I. (2007). Conditional inactivation of Fbxw7 impairs cell-cycle exit during T cell differentiation and results in lymphomagenesis. *J. Exp. Med.* 204, 2875–2888.
- Palomero, T., Lim, W.K., Odom, D.T., Sulis, M.L., Real, P.J., Margolin, A., Barnes, K.C., O’Neil, J., Neuberger, D., Weng, A.P., et al. (2006). NOTCH1 directly regulates c-MYC and activates a feed-forward-loop transcriptional network promoting leukemic cell growth. *Proc. Natl. Acad. Sci. USA* 103, 18261–18266.
- Rajagopalan, H., Jallepalli, P.V., Rago, C., Velculescu, V.E., Kinzler, K.W., Vogelstein, B., and Lengauer, C. (2004). Inactivation of hCDC4 can cause chromosomal instability. *Nature* 428, 77–81.
- Real, P.J., Tosello, V., Palomero, T., Castillo, M., Hernando, E., de Stanchina, E., Sulis, M.L., Barnes, K., Sawai, C., Homminga, I., et al. (2009). Gamma-secretase inhibitors reverse glucocorticoid resistance in T cell acute lymphoblastic leukemia. *Nat. Med.* 15, 50–58.
- Reavie, L., Della Gatta, G., Crusio, K., Aranda-Orgilles, B., Buckley, S.M., Thompson, B., Lee, E., Gao, J., Bredemeyer, A.L., Helminck, B.A., et al. (2010). Regulation of hematopoietic stem cell differentiation by a single ubiquitin ligase-substrate complex. *Nat. Immunol.* 11, 207–215.
- Reavie, L., Buckley, S.M., Loizou, E., Takeishi, S., Aranda-Orgilles, B., Ndiaye-Lobry, D., Abdel-Wahab, O., Ibrahim, S., Nakayama, K.I., and Aifantis, I. (2013). Regulation of c-Myc ubiquitination controls chronic myelogenous leukemia initiation and progression. *Cancer Cell* 23, 362–375.
- Rhodes, D.R., Yu, J., Shanker, K., Deshpande, N., Varambally, R., Ghosh, D., Barrette, T., Pandey, A., and Chinnaiyan, A.M. (2004). Large-scale meta-analysis of cancer microarray data identifies common transcriptional profiles of neoplastic transformation and progression. *Proc. Natl. Acad. Sci. USA* 101, 9309–9314.
- Rossi, D., Trifonov, V., Fangazio, M., Brusca, G., Rasi, S., Spina, V., Monti, S., Vaisitti, T., Arruga, F., Famà, R., et al. (2012). The coding genome of splenic marginal zone lymphoma: activation of NOTCH2 and other pathways regulating marginal zone development. *J. Exp. Med.* 209, 1537–1551.
- Sharma, V.M., Calvo, J.A., Draheim, K.M., Cunningham, L.A., Hermance, N., Beverly, L., Krishnamoorthy, V., Bhasin, M., Capobianco, A.J., and Kelliher, M.A. (2006). Notch1 contributes to mouse T-cell leukemia by directly inducing the expression of c-myc. *Mol. Cell. Biol.* 26, 8022–8031.
- Soucek, L., Whitfield, J., Martins, C.P., Finch, A.J., Murphy, D.J., Sodir, N.M., Karnezis, A.N., Swigart, L.B., Nasi, S., and Evan, G.I. (2008). Modelling Myc inhibition as a cancer therapy. *Nature* 455, 679–683.
- Thompson, B.J., Buonamici, S., Sulis, M.L., Palomero, T., Vilimas, T., Basso, G., Ferrando, A., and Aifantis, I. (2007). The SCFFBW7 ubiquitin ligase complex as a tumor suppressor in T cell leukemia. *J. Exp. Med.* 204, 1825–1835.
- Thompson, B.J., Jankovic, V., Gao, J., Buonamici, S., Vest, A., Lee, J.M., Zavadil, J., Nimer, S.D., and Aifantis, I. (2008). Control of hematopoietic stem cell quiescence by the E3 ubiquitin ligase Fbw7. *J. Exp. Med.* 205, 1395–1408.
- Tsunematsu, R., Nakayama, K., Oike, Y., Nishiyama, M., Ishida, N., Hatakeyama, S., Bessho, Y., Kageyama, R., Suda, T., and Nakayama, K.I. (2004). Mouse Fbw7/Sel-10/Cdc4 is required for notch degradation during vascular development. *J. Biol. Chem.* 279, 9417–9423.
- Wang, Z., Inuzuka, H., Zhong, J., Wan, L., Fukushima, H., Sarkar, F.H., and Wei, W. (2012). Tumor suppressor functions of FBW7 in cancer development and progression. *FEBS Lett.* 586, 1409–1418.
- Welcker, M., and Clurman, B.E. (2007). Fbw7/hCDC4 dimerization regulates its substrate interactions. *Cell Div.* 2, 7.
- Weng, A.P., Ferrando, A.A., Lee, W., Morris, J.P., 4th, Silverman, L.B., Sanchez-Izarray, C., Blacklow, S.C., Look, A.T., and Aster, J.C. (2004). Activating mutations of NOTCH1 in human T cell acute lymphoblastic leukemia. *Science* 306, 269–271.
- Weng, A.P., Millholland, J.M., Yashiro-Ohtani, Y., Arcangeli, M.L., Lau, A., Wai, C., Del Bianco, C., Rodriguez, C.G., Sai, H., Tobias, J., et al. (2006). c-Myc is an important direct target of Notch1 in T-cell acute lymphoblastic leukemia/lymphoma. *Genes Dev.* 20, 2096–2109.
- Zhang, J., Ding, L., Holmfeldt, L., Wu, G., Heatley, S.L., Payne-Turner, D., Easton, J., Chen, X., Wang, J., Rusch, M., et al. (2012). The genetic basis of early T-cell precursor acute lymphoblastic leukaemia. *Nature* 481, 157–163.
- Zuber, J., Shi, J., Wang, E., Rappaport, A.R., Herrmann, H., Sison, E.A., Magoon, D., Qi, J., Blatt, K., Wunderlich, M., et al. (2011). RNAi screen identifies Brd4 as a therapeutic target in acute myeloid leukaemia. *Nature* 478, 524–528.

## EXTENDED EXPERIMENTAL PROCEDURES

### Genotyping

Positive ES cell clones were screened by PCR and Southern blot prior to blastocyst injection. Strains were backcrossed to wild-type C57/BL6 strains for several generations. The following primer sequences were used for genotyping: *Fbxw7* knockin STOP F: ACTG CATTCTAGTTGTGGTTTGTCC; PT2 R: GCATACAGTAGAAGTGTGCCATA; In11 F: TCTAAATCACTGAGCCATCTCC; Ex11 R: ATCTGACACCATCACTACCT; *Eef1a1* hFBXW7 $\alpha$  R465C Eef1 in1-2 F: TGCCTGCGTGGAAAGATGGC; SA R: AGGAAACCCTG GACTACTGC; Eef1 inF: TATCGGCCGCAATAGTCAC; hW7 R: GGAAGGGTTACCTCTCAG.

### Flow Cytometric Analysis and Cell Sorting

Single cell suspensions were derived from bone marrow (femur and tibia), spleen and thymus from adult (>6 weeks) mice and red blood cells were lysed with ACK buffer. Nonspecific antibody binding was blocked by incubation with 20  $\mu$ g/ml Rat IgG (Sigma-Aldrich) for 15 min. Cells were incubated with primary and secondary antibodies for 30 min on ice. All antibodies were purchased from BD-PharMingen, eBioscience or BioLegend. We used the following fluorochrome or biotin conjugated anti-mouse antibodies: CD117 (2B8), Sca-1 (D7), CD11b (M1/70), Gr-1 (RB6-8C5), TER-119, CD3 (145-2C11), CD127 (A7R34), CD4 (RM4-5), CD8 (53-6.7), CD150 (9D1), B220 (RA3-6B2), CD48 (HM481), CD45.1 (A20), CD45.2 (104), CD25 (PC61), CD44 (IM7), TCR $\beta$  (H57-597). Bone marrow mature lineage markers were defined as CD11b, Gr-1, TER-119, CD4, CD8, CD3, and B220. Stained cells were quantified using a BD Fortessa analyzer or isolated with a MoFlo cell sorter (Beckman Coulter) or BD ARIA II. Human CD34<sup>+</sup> cells were isolated directly from xenografts using the EasySep Human CD34 Positive Selection Kit (STEMCELL Technologies). FlowJo software (Tree Star) was used to generate FACS plots, histograms and calculate mean fluorescence intensities.

### Microarray and Gene Set Enrichment Analysis

Total RNA was extracted using the RNeasy Plus Micro kit (QIAGEN). RNA quantification and quality was determined using an Agilent 2100 Bioanalyzer. The Ovation RNA Amplification System V2 (NuGEN) kits were used for amplification. Amplified RNA was labeled and hybridized to the Mouse 430.2 microarrays (Affymetrix). The Affymetrix gene expression profiling data were normalized using the GC-RMA algorithm. The gene expression intensity presentations were generated with Multi Experiment Viewer software. Gene set enrichment analysis was performed using gene set as permutation type, 1,000 permutations and log<sub>2</sub> ratio of classes as metric for ranking genes. Gene sets used in this study were identified from the Molecular Signatures Database (MSigDB Curated v3.0) or have been previously published (Kim et al., 2008).

### Quantitative Real-Time PCR

For mRNA quantification, total RNA was isolated from cells using the RNeasy Plus Mini Kit (QIAGEN). RNA was quantified by absorbance at A260 nm and 1  $\mu$ g of total RNA used for cDNA synthesis using Superscript III first strand synthesis kit (Invitrogen). For ChIP assays, decrosslinked chromatin immunoprecipitates and corresponding whole cell extracts were compared using Rabbit IgG as a negative control. Real time PCR reactions were carried out using SYBR Green Master Mix (Roche) and run with a Lightcycler 480 II (Roche). The following primer sequences were used for cDNA quantification: *Fbxw7* (mouse) for CGGACTCTCAAAGTGTGG, rev CCTCCTGCCATCATACTG; *Myc* (mouse) for ACAGGACTCCCCAGGCTCCG, rev CGTGGCTGTCTGCGGGGTTT; *FBXW7* (human) for GTGATAGAACCCAGTTTCA, rev CTCAGCCAAAATTCTCCAG; *MYC* (human) for GCTGCTTAGACGCTGGATTT, rev CGAGGTCATAGTTTCTGTTGG. For ChIP assays: ACTB\_ex4 for AGCGCGGCTACAGCTTCA, rev CGTAGCACAGCTTCTCCT TAATGTC; BCL2enh for CTCACACCAAACAGCTTGCC, rev ACAGCAACTACACAGGACGG; BCL2pro for GGGCACAGGCAT GAATCTCT, rev TCCTTCATCGTCCCCTCTCC; IL7Renh for AGCCATGTGTGAGAAGTCGG, rev CCCCACCCTATTGTTTCCCC; IL7Rpro for AAGCACAGTAAGTGTGGGGG, rev GCTGCTGTAAGCAGAGGTCA; MYCenh for TAGACAGGCAGCACTCTCCT, rev CCTAAGAGGCGCGTGATAC; TCRAenh for AAGTCTCCCCTCTCCCTCCA, rev CTTCTGCGGGAGAGCTTCAA.

### In Vitro Colony-Forming Assays

Live Lin<sup>-</sup>c-kit<sup>+</sup>Sca1<sup>+</sup> (LSK) cells sorted from bone marrow of *Fbxw7*<sup>+/+</sup>Mx1Cre<sup>+</sup>, *Fbxw7*<sup>F/F</sup>Mx1Cre<sup>+</sup> or *Fbxw7*<sup>mut/+</sup>Mx1Cre<sup>+</sup>, 2 weeks following pl:pC injection, and were seeded in triplicate (250 cells/well) and cultured in cytokine-supplemented methylcellulose medium (MethoCult 3434; STEMCELL Technologies). Colonies were counted on day 8, then were isolated, replated (1,000 cells/well) and cultured for another 8 days.

### Protein Purification and Quantification

To quantify protein stability in Notch1 T-ALL cells, total splenocytes (>95% GFP<sup>+</sup>) from transplant recipients were treated with 100  $\mu$ g/ml cyclohexamide (Sigma) for the length of time indicated and lysed in RIPA buffer. 50  $\mu$ g of whole cell lysate was loaded per lane, separated on a 4%–12% NuPage Bis-Tris polyacrylamide gel (Invitrogen) and transferred to PVDF membrane. For SCF-FBXW7 dimer tandem immunoprecipitation, HEK293 cells were transfected with 10  $\mu$ g of each pCDNA3.1 vector per 10 cm dish. Two days later, cells were treated with proteasome inhibitor (MG132, 20  $\mu$ M) for 3h and cells were lysed in 150 mM NaCl, 50 mM Tris (pH 8.0), 1% NP-40 supplemented with complete protease and phosphatase inhibitors (Roche) and briefly sonicated. Strep-II tagged proteins were affinity purified from cleared lysates with Strep-Tactin resin, washed thoroughly and eluted in desthiobiotin

(IBA Life Sciences). The eluted protein complexes were then incubated with anti-HA affinity gel (Sigma), washed thoroughly and boiled in SDS loading buffer with 1%  $\beta$ -mercaptoethanol for PAGE separation. The following primary antibodies were used for western blotting: c-Myc (Cell Signaling, 9402), Cleaved Notch1 Val1744 (Cell Signaling), HA (Santa Cruz), StrepMAB-classic (IBA), p53 (Leica, CM5), mTOR (Cell Signaling, 2972), SREBP1 (Santa Cruz), Cyclin E (Abcam, ab7959) Skp1 (52/p19, BD), and  $\beta$ -actin (C4, Millipore). Horseradish peroxidase (HRP) conjugated anti-mouse or anti-rabbit secondary antibodies (GE Healthcare) were added and blots were developed with SuperSignal West Pico ECL Kit (Thermo) and exposed to film.

### In Vitro Ubiquitylation Assays

c-Myc in vitro ubiquitylation was performed by using c-Myc (0.4  $\mu$ l) translated by TNT SP6 coupled wheat germ system in the presence of GSK3 $\beta$  (10 ng/ $\mu$ l), E1 (100nM), UbcH3 (10 ng/ $\mu$ l), UbcH5c (10 ng/ $\mu$ l), ubiquitin (2.5  $\mu$ g/ $\mu$ l), 1  $\mu$ M Ubiquitin Aldehyde and 1  $\mu$ l of wild-type or mutated Fbxw7 translated by TNT T7 coupled wheat germ system in a total volume of 10  $\mu$ l. Reaction buffer was 50mM Tris-HCl, 10mM MgCl<sub>2</sub>, 0.6 mM DTT and 4mM ATP. Reactions were incubated for 60 min at 30 C.

### Metaphase Preparation and Fluorescence In Situ Hybridization

Primary *Fbxw7* mutant T-ALL cells were grown in complete RPMI media for 4 h and exposed to colcemid (0.04  $\mu$ g/ml, GIBCO, KaryoMAX Colcemid Solution) for 2 hours at 37 °C. Cells were incubated in hypotonic solution (75 mM KCl) for 15 min at 37 °C, fixed in 75% methanol/25% acetic acid and washed three times in the fixative solution. Cell suspensions were dropped onto prechilled glass slides and air-dried. Chromosomes were stained using the 21XMouse Multicolor FISH Probe Kit according to manufacturer instructions (MetaSystems), and mounted in ProLong Gold (Invitrogen) containing 4',6-diamidino-2-phenylindole (DAPI) to counterstain total DNA. Metaphases were identified using an Isis Fluorescence Imaging System with Metafer Slide Scanning Platform and MSearch algorithm (MetaSystems). Karyotypes were determined with the Isis software package.

### Primary Human T-ALL Samples and In Vitro Drug Treatments

Samples were collected by collaborating institutions with informed consent and analyzed under the supervision of the Columbia University Medical Center Institutional Review Board. Cells were cultured in MEM $\alpha$  medium supplemented with 10% fetal bovine serum (StemCell Technologies, Inc. #06400), 10% human AB<sup>+</sup> serum (Invitrogen), 1% penicillin/streptomycin, 1% GlutaMAX, human IL-7 (R&D Systems; 10 ng/ml), human Flt3-ligand (Peprotech; 20 ng/ml), human SCF (Peprotech; 50 ng/ml) and insulin (Sigma; 20 nmol/L) on a feeder layer of irradiated MS5 stromal cells overexpressing Delta-like 1 (DLL1), as previously described (Armstrong et al., 2009). Primary cultures were treated for 72 hr with 500nM JQ1 (Cayman Chemical), CPI203 (Constellation Pharmaceuticals) or vehicle (DMSO) and cell viability was analyzed both manually and using the BD cell viability kit with liquid counting beads (BD Bioscience) in combination with the anti-human CD45 staining to gate out stromal cells.

### Histology and Immunohistochemistry

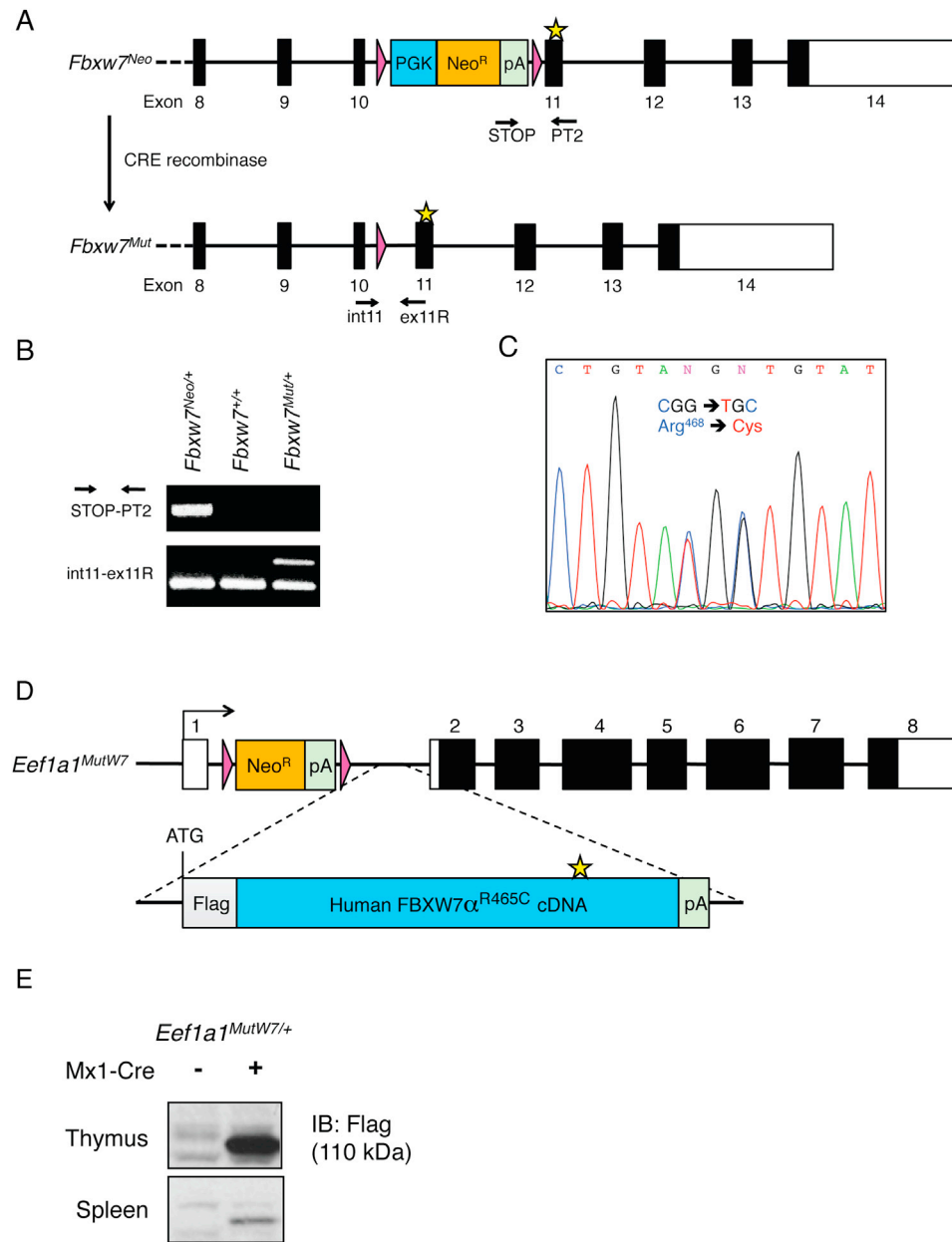
Peripheral blood smears were briefly fixed in methanol and stained with Wright-Giemsa solution (Fisher). Slides were rinsed with water, dried, mounted with Cytoseal 60 and coverslipped. Tissues were dissected from mice for fixation overnight in 10% formalin. Fixed tissues were dehydrated and embedded in paraffin for sectioning. 5  $\mu$ m paraffin sections were prepared and stained with hematoxylin and eosin (Leica Autostainer XL). For immunohistochemistry, sections were dewaxed by immersion in xylene and hydrated by serial immersion in 100% ethanol, 95% ethanol, 70% ethanol and distilled water. Antigen retrieval was performed by boiling for 15 min in 0.01M citrate (pH 6.0). Primary Ki67 antibody (Epitomics, Clone SP6) was added 1:250 in PBS + 1% BSA and incubated for 1 hr at room temperature. Slides were rinsed in PBS and peroxidase activity was detected using Envision+ DAB Rabbit Kit (Dako). Nuclei were counterstained with hematoxylin for 2 min and slides were rinsed in water, dehydrated, mounted with Permount (Fisher) and coverslipped. Light microscopy was performed using a Zeiss Axio Observer microscope.

### Array CGH Analysis

Genomic DNA was isolated from spleen of primary T-ALL recipients and paired with genomic DNA from bone marrow donor tail biopsies as a reference. Paired DNA samples were differentially labeled and hybridized to Mouse 3  $\times$  720 Whole Genome Tiling Arrays (Roche Nimblegen). Raw data were spatially corrected using locally weighted polynomial regression (Loess) and signal intensities normalized to one another using qspline normalization. Copy number variations were identified using CGH-segMNT analysis.

### RNaseq Library Preparation and Analysis

Whole RNA was extracted from 1 million CUTLL1 cells per replicate using TriZol reagent (Invitrogen) according to the manufacturer's protocol. Whole RNA was treated with DNase for 30 min (Invitrogen) and purified with RNA clean & concentrator columns (Zymo). Ribosomal RNA was depleted using RiboZero magnetic kit (Epicenter) according to manufacturer's protocol. cDNA preparation and strand-specific library construction was performed using the dUTP method as described by Zhong and colleagues (<http://dx.doi.org/10.1101/pdb.prot5652>). Libraries were sequenced on the Illumina HiSeq 2000 using 50bp single end reads. Base calling and quality filtering was performed as in ChIP-seq data. Fastq files were aligned to Hg19 using TopHat allowing 2 mismatches. Differential expression tests were done using the Cuffdiff module of Cufflinks against the RefSeq annotation. We used FDR (0.05) corrected p value of 0.05 as a cutoff for significance.



**Figure S1. Generation of Inducible *Fbxw7* Mutant Knockin Animals, Related to Figures 1 and 2**

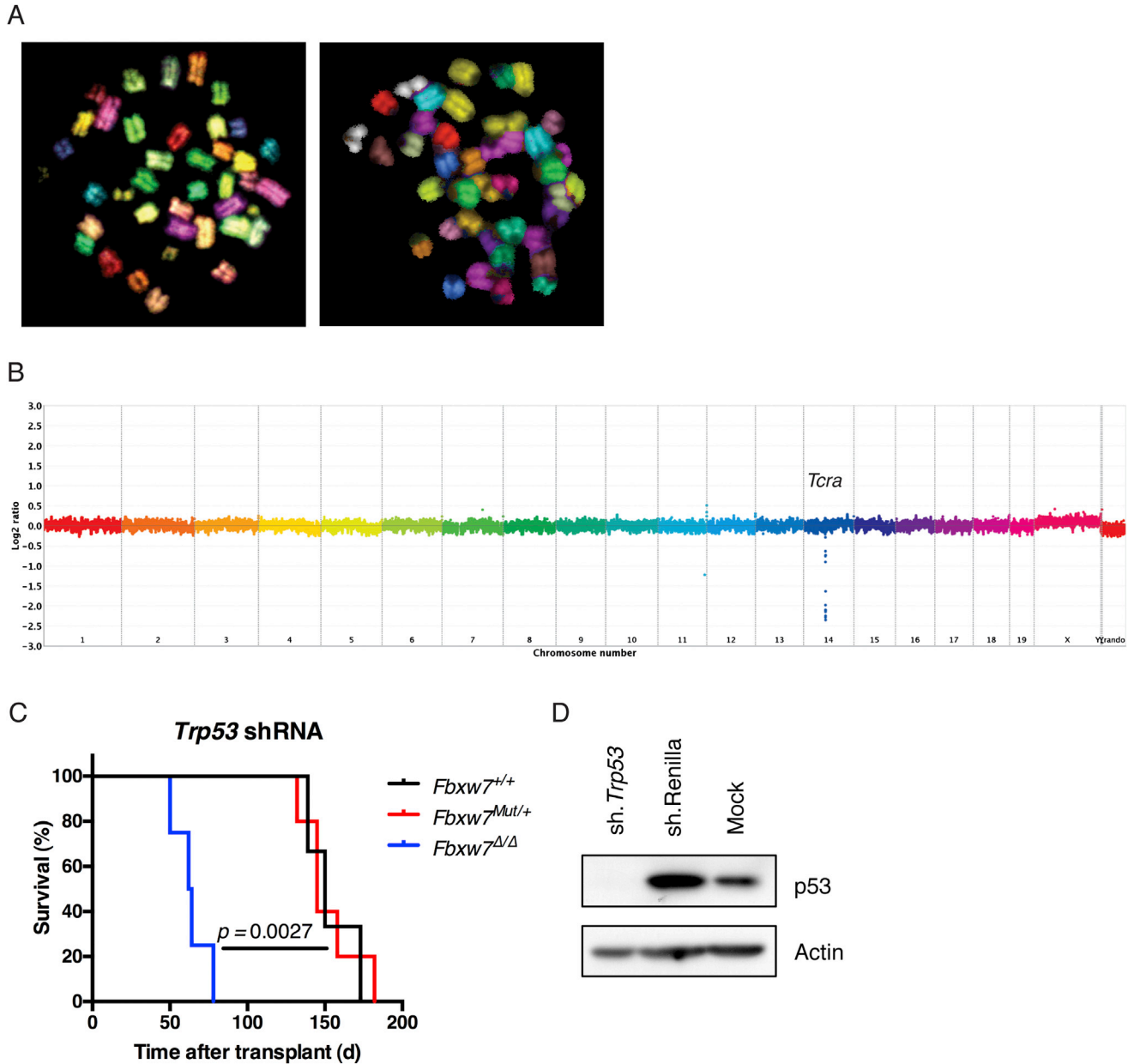
(A) Schematic depiction of conditionally activated *Fbxw7* mutant allele before and after Cre-mediated recombination.

(B) Polymerase chain reaction (PCR) of genomic DNA prepared from thymus of *Fbxw7* mutant or wild-type 2 weeks post pl:pC injection, demonstrating loss of PGK-Neo-STOP cassette and appearance of recombinant product.

(C) Sequence chromatogram showing DNA substitutions in complementary DNA (cDNA) (resulting in a R468C substitution) prepared from *Fbxw7*<sup>mut/+</sup> c-kit<sup>+</sup> bone marrow progenitors.

(D) Schematic of mutant (R465C) human FBXW7 alpha cDNA knocked-in to *Eef1a1* locus.

(E) Immunoblot for Flag-tagged human FBXW7 mutant in spleen and thymus in *Eef1a1*<sup>mutW7/+</sup> following pl:pC induction.



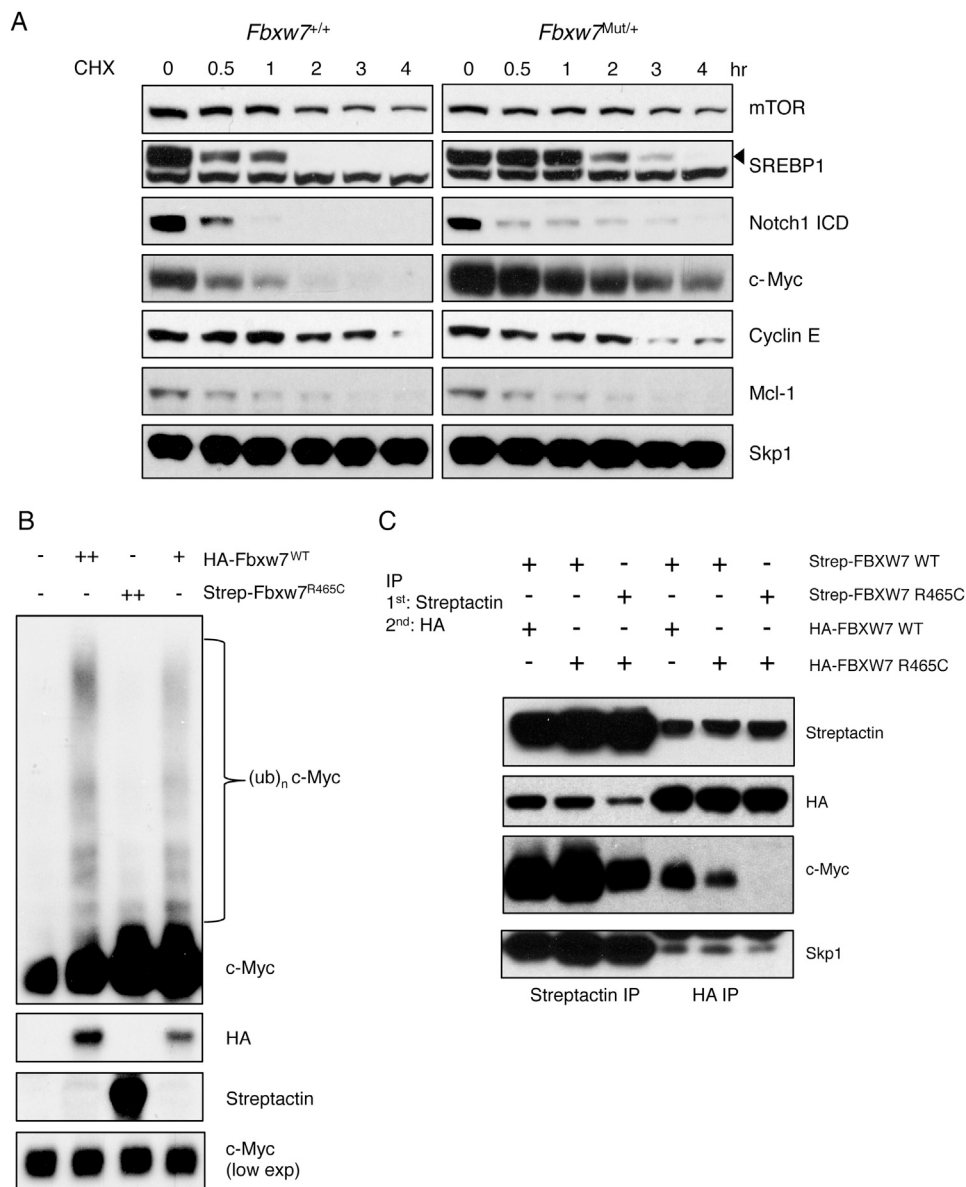
**Figure S2. No Evidence for Genomic Instability in the FBXW7 Mutant Leukemia, Related to Figure 2**

(A) Representative images of metaphases from two separate *Fbxw7* mutant T-ALL showing pseudo-coloring of unique chromosomes as determined by m-FISH analysis. 19 pairs of autosomes and two X chromosomes were identified in each, consistent with a normal mouse karyotype.

(B) Rainbow plot of normalized and averaged array CGH data measuring DNA content genome-wide from an *Fbxw7*-mutant T-ALL when compared to corresponding donor tail biopsy.

(C) Kaplan-Meier curve depicting survival of recipient mice transplanted with bone marrow from *Fbxw7* $^{\Delta/\Delta}$  (*Fbxw7* $^{F/F}Mx1Cre$ +), wild-type or mutant mice transduced with retrovirus expressing a short-hairpin RNA targeting *Trp53* (sh. *Trp53*). \*\* $p = 0.036$ , as determined by Mantel-Cox log-rank test.

(D) Immunoblot for p53 protein in whole-cell lysates of sorted (GFP+) wild-type c-kit $^+$  bone marrow cells 72h following transduction with the retroviral sh. *Trp53* construct used in (c) or an shRNA targeting the Renilla luciferase gene. Uninfected cells (mock) are also shown as a control.

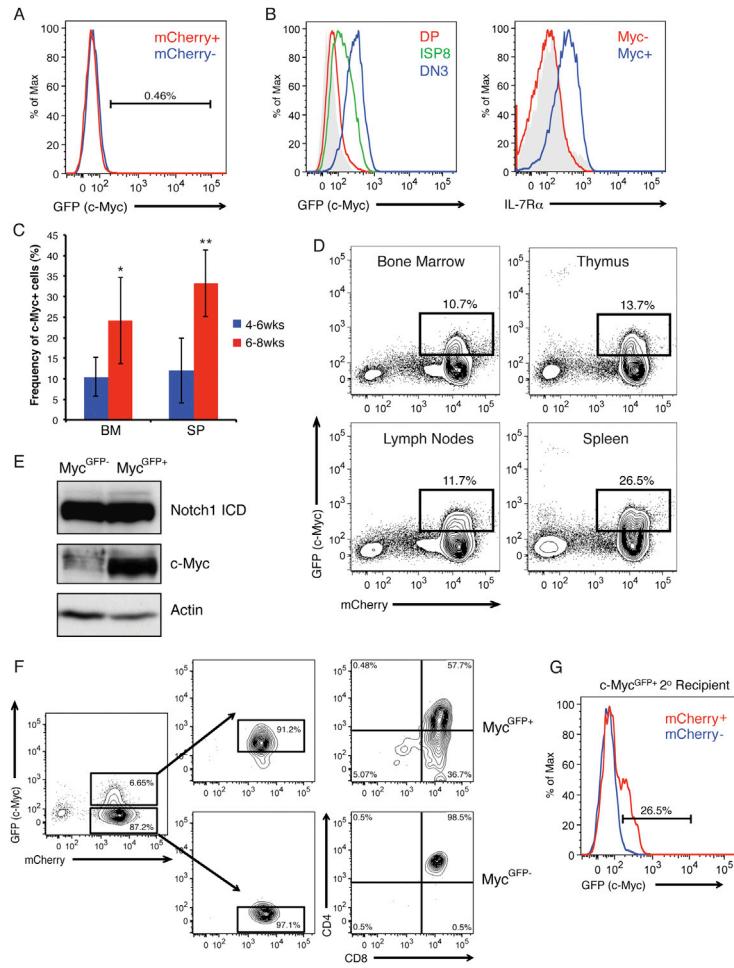


**Figure S3. *Fbxw7* Mutations Confer Enhanced c-Myc Stability through Loss-of-Substrate Interaction and Ubiquitylation by SCF Complex, Related to Figure 3**

(A) Stability of *Fbxw7* protein substrates was determined by immunoblot from *Fbxw7* wild-type or mutant T-ALL cells treated ex vivo with 100  $\mu$ g/ml cyclohexamide for the indicated length of time.

(B) c-Myc was translated in vitro using wheat germ extracts and subjected to in vitro ubiquitination reactions in the presence of GSK3 $\beta$ . Wheat germ extract containing Strep-II tagged *Fbxw7* or HA-tagged *Fbxw7* R465C was added as indicated.

(C) Tandem affinity purification of SCF-*Fbxw7* dimers in HEK293 cells. Strep-II or HA tagged human *Fbxw7* (WT or R465C) was cotransfected and affinity purified sequentially from whole-cell lysates using Strep-Tactin resin and anti-HA beads. Coimmunoprecipitation of endogenous c-Myc and Skp1 was quantified using protein immunoblot.



**Figure S4. Myc<sup>GFP+</sup> LICs Express Unique Surface Markers and Can Be Isolated from Primary Leukemias to Regenerate Tumors upon Transplantation, Related to Figure 3**

(A) Histogram showing overlay of c-Myc<sup>GFP</sup> expression in *Fbxw7* wild-type Notch1ΔE transduced (mCherry<sup>+</sup>) and untransduced (mCherry<sup>-</sup>) cells in peripheral blood of recipient mice, 3 weeks post transplant.

(B) c-Myc<sup>GFP</sup> expression in splenocytes, gated on mCherry<sup>+</sup> and defined phenotypically as DP (CD4<sup>+</sup>CD8<sup>+</sup>), ISP8 (CD4<sup>-</sup>CD8<sup>+</sup>TCRαβ<sup>-</sup>) or DN3 (CD4<sup>-</sup>CD8<sup>-</sup>CD25<sup>hi</sup>) (left panel). CD127 (IL-7Rα) surface expression in mCherry<sup>+</sup>c-Myc<sup>GFP+</sup> or mCherry<sup>+</sup>c-Myc<sup>GFP-</sup> splenocytes (right panel). mCherry<sup>-</sup> splenocytes are shown in solid gray as a reference.

(C) Frequency of Myc<sup>GFP+</sup> cells within the total mCherry<sup>+</sup> population in bone marrow and spleen in cohorts of recipient animals sacrificed between 4–6 weeks or 6–8 weeks post transplant (Mean ± SD shown. N = 5, \*p = 0.041, \*\*p = 0.0061).

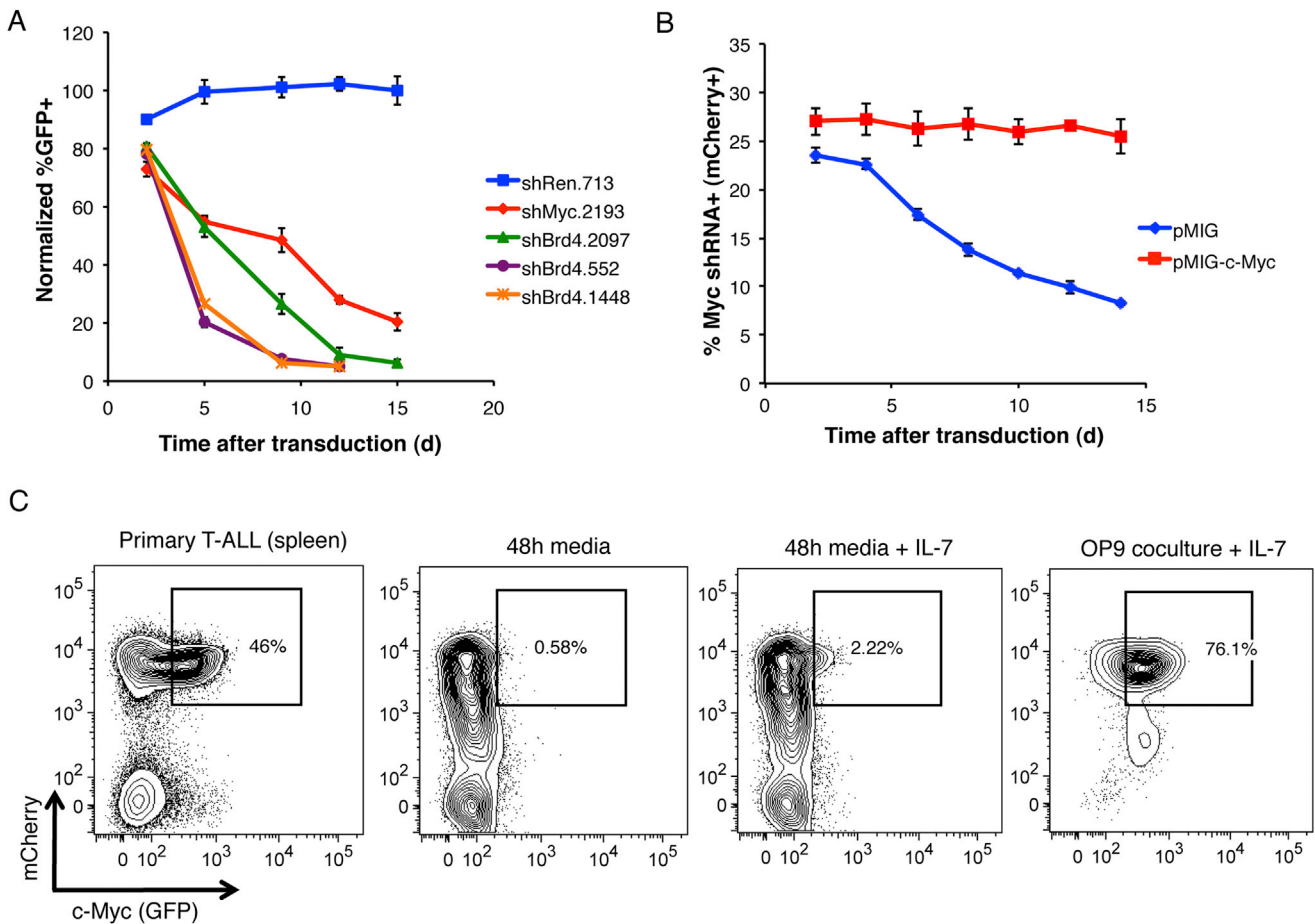
(D) FACS plots depicting mCherry expression (Notch1ΔE transduced) and Myc<sup>GFP</sup> expression in hematopoietic and lymphoid organs from the same mouse 7 weeks posttransplant. Frequency of mCherry<sup>+</sup>Myc<sup>GFP+</sup> cells in each tissue is shown.

(E) c-Myc and intracellular Notch1 ICD protein abundance determined by immunoblot in sorted c-Myc<sup>GFP+</sup> or c-Myc<sup>GFP-</sup> tumor populations.

(F) Sorting scheme for purifying c-Myc<sup>GFP</sup> positive and negative cells from the bulk Notch1ΔE-transduced population. c-Myc<sup>GFP+</sup> or c-Myc<sup>GFP-</sup> cells were re-analyzed after sorting for expression of mCherry, c-Myc<sup>GFP</sup>, CD4 and CD8.

(G) Histogram showing overlay of c-Myc<sup>GFP</sup> expression in mCherry<sup>+</sup> and mCherry<sup>-</sup> splenocytes in secondary recipients transplanted with sorted c-Myc<sup>GFP+</sup> cells.



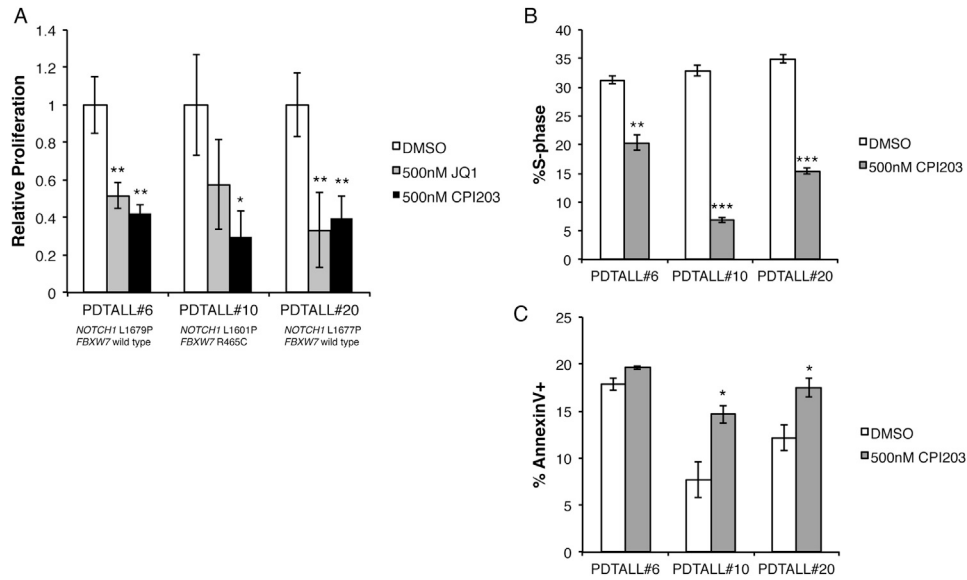


**Figure S5. Silencing of *Myc* or *Brd4* Inhibits Growth of Mouse T-ALL Line, Related to Figures 4 and 6**

(A) Loss of representation assay tracking frequency of mouse 720 T-ALL cells transduced with retroviral vectors containing an shRNA targeting Renilla luciferase, *Brd4*, or *Myc* and a GFP reporter over 2 weeks in culture.

(B) Frequency over time of 720 cells transduced with both an shRNA targeting *Myc* with or without a nontargeted cDNA of c-Myc. Mean  $\pm$  SD of 3 replicates shown for each time point in (A) and (B).

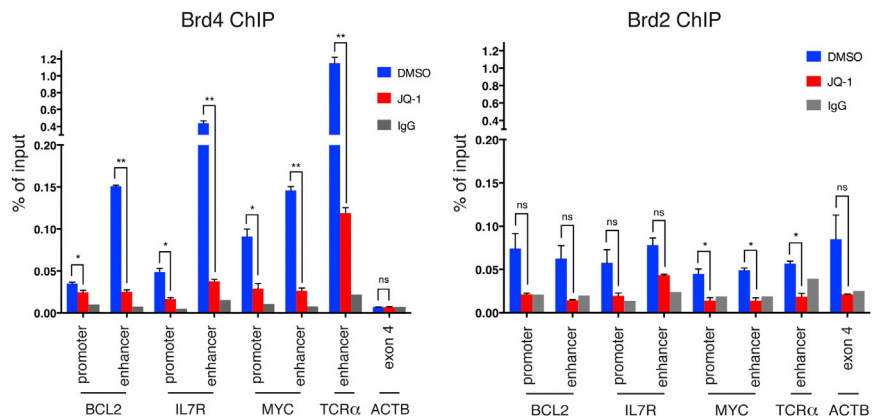
(C) FACS diagrams of primary splenocytes from a mouse transplanted with a Notch1 $\Delta$ E ires mCherry *Myc*<sup>GFP</sup> T-ALL analyzed directly ex vivo (left), after 2 days in liquid culture  $\pm$  5 ng ml<sup>-1</sup> IL-7 (middle) or after 2 weeks of coculture with OP9 stromal line + 5 ng ml<sup>-1</sup> IL-7 (right). Gates show frequency of mCherry<sup>+</sup>*Myc*<sup>GFP+</sup> cells under each condition.



**Figure S6. Selective BET Bromodomain Inhibitors Restrain Growth of Primary Human T-ALL, Related to Figures 5 and 6**

(A) Relative growth of primary human T-ALL samples treated with 500nM JQ1, 500nM CPI203 or an equivalent concentration of vehicle (DMSO) for 72 hr in vitro. Mutation status of *NOTCH1* and *FBXW7* for each patient is shown.

(B and C) Cell cycle progression (BrdU incorporation after 1h pulse) (B) and apoptosis (AnnexinV) (C) was measured in the same samples shown in (A) treated with either 500nM CPI203 or vehicle. Mean  $\pm$  SD of 3 biological replicates is shown. \* $p < 0.05$ , \*\* $p < 0.01$ , \*\*\* $p < 0.001$ .



**Figure S7. Loss of Brd4 Binding at Gene Promoters and Enhancers upon Treatment with JQ1, Related to Figure 7**

Chromatin immunoprecipitation was performed using antibodies specific to either Brd4 (left) or Brd2 (right) in CUTLL1 cells treated for 12h with either JQ1 or an equivalent concentration of vehicle (DMSO). Enrichment at selected gene loci was determined by real-time quantitative PCR and shown relative to input genomic DNA. Mean  $\pm$  SD of 3 biological replicates is shown. \* $p < 0.05$ , \*\* $p < 0.001$ .